

ANNEXLYSE: VALIDATION OF YAW MODELS, ON BASIS OF DETAILED AERODYNAMIC MEASUREMENTS ON WIND TURBINE BLADES

J.G. Schepers

Acknowledgement

Arne van Garrel is acknowledged for performing the AWSM calculations.

Financial support for this research was given in part by the Netherlands Agency for Energy and the Environment, NOVEM under contract 2020-01-13-10-003. Additional support was given by the Dutch Ministry of Economic Affairs.

Abstract

In this report an analysis is made of measured local aerodynamic loads on wind turbine blades at yawed conditions. The measured loads are compared with results from the wind turbine design code PHATAS-IV. The aerodynamic model in PHATAS-IV is based on the blade element momentum model, with correction formula for yawed conditions. The measured data are also compared with the results from the newly developed free wake lifting line model AWMS.

Keywords

Yaw aerodynamics of wind turbines

Validation of wind turbine design codes

CONTENTS

SUMMARY	5
SYMBOLS	7
1. INTRODUCTION	9
2. HISTORIC PERSPECTIVE OF YAW MODELLING	12
3. SELECTION OF CAMPAIGNS	17
3.1 Selected ECN campaigns	17
4. ANALYSIS OF RESULTS BY MEANS OF PHATAS CALCULATIONS	19
5. AWSM CALCULATIONS	30
6. CONCLUSIONS	32
REFERENCES	33
APPENDIX A. AZIMUTHALLY BINNED AVERAGED VALUES ON ECN TURBINE	35
EXECUTIVE SUMMARY	63

SUMMARY

This report describes an analysis of aerodynamic measurements on wind turbines at yawed conditions. The analysis is performed within the Dutch national project 'Annexlyse' in which the measurements from the IEA Annex XVIII project are investigated. In IEA Annex XVIII local aerodynamic loads (i.e. pressure distributions and the resulting aerodynamic forces) were measured at different radial positions on a rotorblade.

The main emphasis in the present investigation was on the analysis of the axial load distribution over the rotorplane at yawed conditions, i.e. the variation of the axial force of a blade section with the azimuth angle. This variation is partly determined by the variation of the induced velocity (and consequently the variation of inflow velocity) over the rotorplane, which results from the skewed wake geometry. Commonly it is assumed that the inflow distribution is sinusoidally distributed over the azimuth angle, with the maximum value at the upwind side of the rotorplane leading to a stabilizing (restoring) yawing moment contribution over the entire blade.

However, the yaw model which is implemented in the PHATAS-IV code is not based on such sinusoidal distribution. It has used information from wind tunnel measurements of the inflow distribution in the rotorplane of model rotor. These measurements showed that at the tip of a rotor blade, the inflow distribution is more or less sinusoidal with the maximum velocity at the upwind side of the rotorplane, but near the root the maximum velocity occurs at the downwind side of the rotorplane. This led to the expectation that the root of a blade can contribute to a destabilizing yawing moment. Unfortunately this could not be extracted from the wind tunnel measurements, where the load distribution was not measured. The advantage of the present IEA Annex XVIII measurements is that they do provide direct information on the load distribution.

The most important conclusion from the present investigation is then the confirmation, that the root of a blade (i.e. the 30% span location), does show the maximum forces to appear at the downwind side of the rotorplane, where at the tip (i.e. at 80% span) the maximum is found at the upwind side of the rotorplane. Hence the root adds a destabilizing yawing moment contribution, where the tip adds a stabilizing yawing moment contribution.

Finally a limited comparison has been made with the newly developed free wake lifting line code AWSM. The AWSM results show a good agreement with the measurements at the 80% section, but at the 30% section there were considerable differences. The explanation for these differences have not been found yet.

SYMBOLS

Quantity	Description	Unit
a	axial induction factor	[-]
B	number of blades	[-]
c	chord	[m]
c_n	normal force coefficient	[-]
c_t	tangential force coefficient	[-]
$C_{D,ax}$	axial force coefficient	[-]
D	rotor diameter	[m]
F_{ax}	axial force	[(k)N]
ibl	blade number	
M_{yaw}	yawing moment	[(k)Nm]
n	normal (to the chord) aerodynamic force at a blade section	[N]
r	radial position (relative to rotor centre)	[m]
R	radius of the rotor	[m]
$shear_{up}$	difference between wind speed at top of rotor plane and wind speed at hub height, defined positive if wind speed increases with height	[m/s]
$shear_{low}$	difference between wind speed at bottom of rotor plane and wind speed at hub height, defined positive if wind speed increases with height	[m/s]
t	tangential (parallel the chord) aerodynamic force at a blade section	[N]
$u_{i,ax}$	axial component of induced velocity	[m/s]
\bar{u}_i	azimuth averaged value of induced velocity	[m/s]
V	local wind speed at blade section	[m/s]
V_{ax}	axial component of wind speed in rotor plane	[m/s]
V_{wind}	free stream wind velocity (usually at hub height)	[m/s]
$V_{wind,ax}$	axial component of free stream wind velocity	[m/s]
$V_{wind,tang}$	tangential component of free stream wind velocity	[m/s]
α	angle of attack	[deg]
ϕ_r	azimuth angle	[deg]
ϕ_y	yaw angle	[deg]
ρ	air density	[kg/m ³]
Ω	rotor speed	[rpm]
θ_{tip}	pitch angle	[deg]
ψ_n	phase of the n^{th} Fourier component of the axial induced velocity	[deg]

Indices	Description
30,60,80	30, 60 and 80% span

1. INTRODUCTION

Modelling of yawed conditions is known to be one of the most difficult topics in wind turbine aerodynamics. In the past, large discrepancies have been found in the prediction of mechanical loads at yawed conditions and in particular the prediction of yawing moments (and stability) suffered from large uncertainties, see [1] and [2].

In this report an investigation on yaw effects is described. The investigation forms part of task 3.4 of the Annexlyse project, sponsored by the Netherlands Agency for Energy and the Environment, NOVEM. The general objective of the Annexlyse project is to analyse the measurements which have been collected within IEA Annex XVIII. In the IEA Annex XVIII project (see www.ecn.nl/wind/other/IEA/index.en.html and [3]), local aerodynamic loads were measured at different radial positions on a rotorblade.

Other investigations from the Annexlyse project (which mainly focus on the IEA Annex XVIII measurements at non-yawed conditions) can be found on the Annexlyse Internet site <http://www.ecn.nl/extranet/annexlys/index.html> and in [4], [5], [6] and [7].

As mentioned above, the present study focusses on the IEA Annex XVIII measurements at yawed conditions. In order to understand these measurements, they have been simulated with the PHATAS-IV code. The main emphasis in the investigation was on the analysis of the axial load distribution over the rotorplane, i.e. the variation of the axial force of a blade section with the azimuth angle. This load distribution determines the yawing stability of a wind turbine, because it yields the load unbalance between the upwind and downwind side of the rotorplane. As such it is extremely important for the stability of free yawing turbines but obviously also for the prediction of fatigue and extreme loads. The load distribution is partly determined by the variation of the induced velocity over the rotorplane, which results from the skewed wake geometry at yawed conditions. Until now, most aerodynamic engineering models assume this variation to be sinusoidal as defined in the EU JOULE projects 'Dynamic Inflow', see [1] and [2]. Such sinusoidal distribution yields a stabilizing (i.e. a restoring) yawing moment contribution for the entire blade.

Within a Dutch national project, see [8], it was shown that this sinusoidal distribution is a rather crude simplification. This was found from wind tunnel velocity measurements, which were carried out in the rotorplane of a model wind turbine. These measurements showed a considerable deviation from the expected sinusoidal inflow distribution. The deviation is caused by velocities which are induced by the root vorticity. The results led (under the assumption of linear aerodynamics) to the suspicion that the yawing moment contribution at the root is destabilizing where it is stabilizing at the tip (though less stabilizing than expected from a sinusoidal model).

The wind tunnel velocity measurements from [8] gave unique information on the inflow variation at yawed conditions but the resulting load distribution, which is determinant for the yawing stability and influenced by additional effects, was not measured. Now, within IEA Annex XVIII the pressure distribution and resulting loads at different radial positions and different azimuth angles have been measured and as such these measurements do offer an opportunity to investigate the load distribution in a direct way. Therefore one of the main objectives of the present

study is to find direct evidence whether the root section of a wind turbine blade can contribute to a destabilizing yawing moment where at the same time the tip section yields a stabilizing yawing moment contribution.

It is important to know that the effects which are investigated at the present study, i.e. the effects from the induced velocity variation, are mainly notable at nominal/high axial induction factors. This usually corresponds to moderate angles of attack. As such they should be distinguished from the yaw effects which are associated to the variations in shed vorticity and which have already been extensively investigated in other projects, see i.e. [9]. The latter are a result of the 1P variation in angle of attack and they will mainly (though not only) be notable at high angles of attack in the form of dynamic stall effects.

The present report is structured in the following way: First a historical overview of yaw modelling is given with a description of the effects which determine the load distribution at yawed conditions, see section 2. Then the selection of suitable measurement campaigns for the study is described in section 3. The analysis of these measurements by means of PHATAS calculations, is described in section 4. The PHATAS code is also used to perform sensitivity studies (among others on the importance of dynamic stall at the selected campaigns). Finally, section 5 compares a limited number of measurements with calculations from the newly developed free wake lifting line code AWSM from ECN, see [10]. This code models the wake and the resulting induced velocities in a physical way, where the PHATAS engineering model is mainly empirical.

For a good understanding of the remaining chapters it is extremely important to absorb the definitions of yaw angle (ϕ_y) and azimuth angle (ϕ_r), as used in this report: The blade azimuth angle is defined as zero for the blade pointing down in vertical position, while the yaw angle is defined positive according to fig. 1.1. It is noted that the definition of the azimuth angle is different from the IEA Annex XVIII definition (which is zero at 12 o'clock'). The present definition is consistent with the one from the Dynamic Inflow projects [1] and [2] and the definition used in [8]. Hence for positive yaw, the upwind side of the rotorplane is between 0 and 180 degrees azimuth and for negative yaw it is between 180 and 360 degrees azimuth.

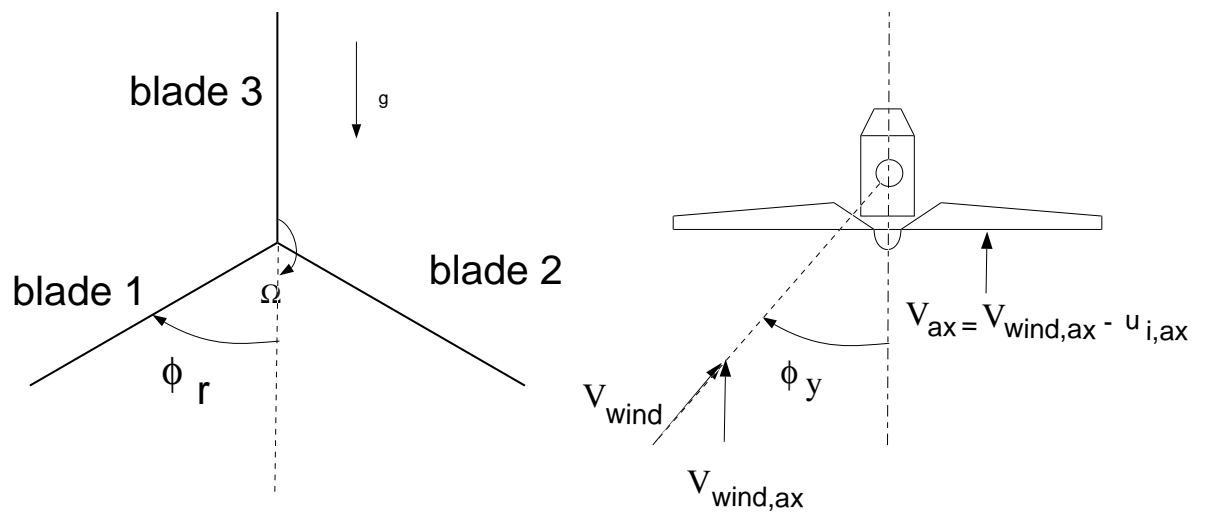


Figure 1.1 Definition of axial induced velocity, yaw angle and azimuth angle

2. HISTORIC PERSPECTIVE OF YAW MODELLING

Until the beginning of the 90's, most blade element methods modelled yawed conditions through the advancing and retreating blade effect only. This effect is explained in figure 2.1 (left).

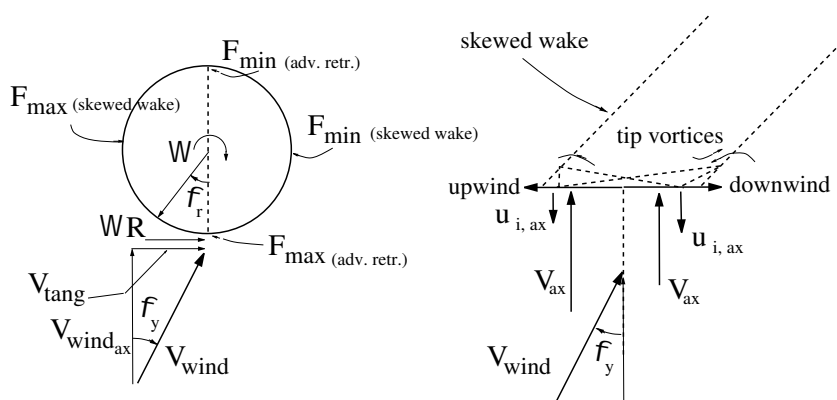


Figure 2.1 *Advancing and retreating blade effect (left) and unbalance in inflow induced by the skewed wake (right)*

For positive yaw, the blade will be retreating in the upper half plane and advancing in the lower half plane with respect to the inplane wind component (V_{tang}). This gives a 1P variation of angle of attack and effective inflow velocity: The advancing and retreating blade effect is symmetric around zero azimuth. In this conventional type of modelling there will only be an aerodynamic tilt moment as a result of yaw, but, averaged over a rotor revolution, not a restoring yaw moment as is measured in reality.

This deficiency was one of the reasons to perform the JOULE projects 'Dynamic Inflow' in which a large number of European institutes participated ([1] and [2]). The projects lasted from 1990 until 1995 and one of the objectives was to develop and validate engineering methods for yawed conditions. In the sequel these models are referred to as 'Dynamic Inflow Engineering models'. The models developed in these projects did not only include the advancing and retreating blade effect, but also the effect of the skewed wake geometry on the inflow distribution, see figure 2.1 (right): The proximity to the rotorplane of the vortices in the wake strongly influences the inflow. The trailing tip vorticity is on the average closer to the downwind side of the rotor plane, which according to the Biot-Savart law results in a larger value of the axial induction velocity $u_{i,ax}$. The higher induced velocity means a lower value of the total axial velocity for the downwind half of the rotorplane and hence lower blade loads in this part. The resulting load unbalance yields a restoring yaw moment.

From helicopter aerodynamics the well known expression from Glauert, [11], is available to model the unbalance in inflow distribution :

$$u_{i,ax} = \bar{u}_i \cdot [1 - K_c f(\frac{r}{R}) \sin \phi_r] \quad (2.1)$$

Such a sinusoidal inflow distribution is found from a simple wake model, in which

the velocities in the rotorplane are induced by a skewed wake which consists of trailed tip vortices only. In the expression derived by Glauert the sinusoidal variation is related to the disc averaged induced velocity \bar{u}_i .

The formula for K_c in equation 2.1 will depend on the shape of the wake. Several expressions for K_c have been developed in helicopter society, see section 6 of [1]. They are all a function of the yaw angle through the wake skew angle χ (the angle between the wake and the rotor axis):

$$\tan\chi = \frac{V_{\text{wind}} \sin\phi_y}{V_{\text{wind}} \cos\phi_y - \bar{u}_i} \quad (2.2)$$

For the radial dependency $f(r/R)$, Glauert proposed a simple linear relation:

$$f\left(\frac{r}{R}\right) = \frac{r}{R} \quad (2.3)$$

All 'Dynamic Inflow engineering models' were basically very similar to equation 2.1 but there were differences in the modelling of the radial dependency ($f(r/R)$) and the dependency on the yaw angle (K_c). Furthermore, the formula has been applied on annular ring level instead of rotor disc level. A representative example of the modelled $V_{ax} - \phi_r$ distribution at positive yaw from one of the 'Dynamic Inflow engineering models' is given in figure 2.2. The figure shows a sinusoidal variation with the maximum value of V_{ax} (And hence the minimum value of $u_{i,ax}$) at the upwind side of the rotorplane at $\phi_r = 90$ degrees, in accordance with the expected inflow unbalance sketched in figure 2.1.

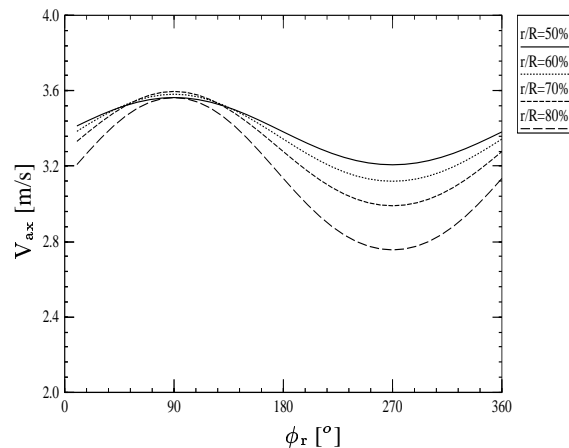


Figure 2.2 *Qualitative sinusoidal $V_{ax} - \phi_r$ behaviour at positive yaw, as predicted by one of the 'Dynamic Inflow engineering models'*

In the Dynamic Inflow projects it turned out that the inclusion of a sinusoidal inflow model, generally spoken, improved the agreement with measured yaw loads considerably in the sense that they have become non-zero and of the correct sign (restoring). Nevertheless large discrepancies were still possible. These were partly attributed to the uncertainties in the modelling of the radial dependency and the yaw angle dependency in the formula for $u_{i,ax}$. This uncertainty is due to the fact that in the Dynamic Inflow projects, measurements of blade root bending moments were available only. These moments consist of an aerodynamic and mass induced

component and they are influenced by the loads over the entire blade spanwise length. Information about the radial and yaw angle dependency of the local aerodynamic loads and the underlying induced velocities can hardly be extracted from such measurements. In order to derive formula for these dependencies in a more straightforward way, it was realised that direct measurements of the inflow distribution at several radial positions were required. This resulted in the Dutch national follow-up project. The project was performed by ECN, where the University of Delft acted as subcontractor, see [8]. The axial flow velocities, V_{ax} (perpendicular to the rotorplane) are measured in the near wake of a wind tunnel rotor with a diameter of 1.2 m. The measurements are done with a hot wire system, 6 cm (10% R) downstream of the rotor plane at four radial positions (50% R, 60% R, 70% R and 90% R) at yaw angles of 30 degrees, 45 degrees and 60 degrees.

A representative result is presented in figure 2.3. In the figure the raw measurement result is presented, as well as a third order Fourier fit according to:

$$V_{ax}(\phi_r) = \sum_{n=1}^{n=3} A_{n,ax} \cdot \cos(n\phi_r - \psi_n) \quad (2.4)$$

Despite the scatter in the raw measurement results, it is remarkable to see the clear trend in the fitted results at all yaw angles. This trend is presented in figure 2.4.

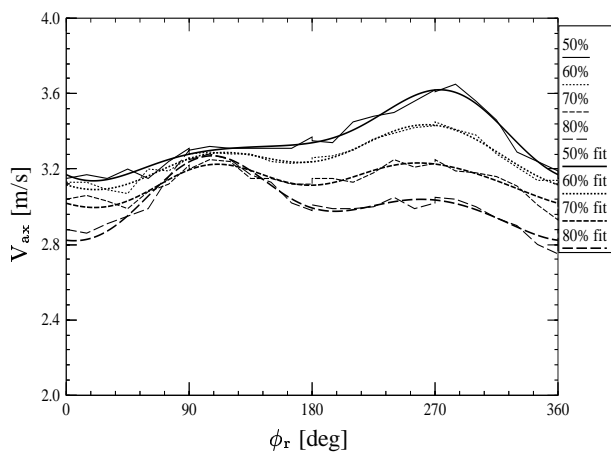


Figure 2.3 *Measured axial velocity at 30 degrees yaw*

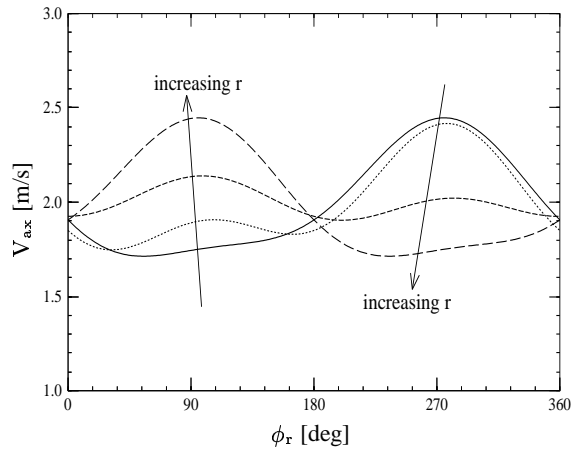


Figure 2.4 Trend of the radial dependency of the axial velocity at a positive yaw angle

If the results from the figures 2.3 to 2.4 are compared with the expected sinusoidal behaviour from figure 2.2 a surprising deviation is apparent:

- At the inner part of the blade, the maximum value of V_{ax} is reached at $\phi_r = 270$ degrees. This implies that the maximum axial velocity is at the downwind part of the rotorplane. Probably the same holds for the loads by which the inner part of the rotor is expected to contribute to a destabilizing yawing moment!
- At the outer part of the blade, the absolute maximum shifts to $\phi_r = 90$ degrees resulting in a stabilizing yawing moment. As a consequence the inflow distribution at the tip becomes more similar to the expected sinusoidal distribution. Nevertheless at $\phi_r = 270$ degrees a local maximum is still apparent. This makes the yawing moment less stabilizing than the yawing moment which results from a sinusoidal inflow distribution.
- The deviation from the expected sinusoidal distribution is explained by root vorticity effects. The sinusoidal velocity distribution is induced by a wake which consists of trailed tip vortices, but obviously the vorticity which is trailed at the root also contributes axial velocities at yawed conditions. In figure 2.5 a calculational result is presented from which the influence of the root vorticity can be extracted.

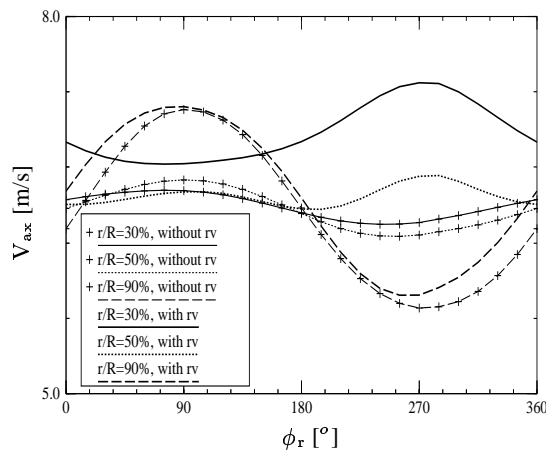


Figure 2.5 JOULE Dynamic Inflow, Tjæreborg turbine: Axial velocity at $\phi_y = +32^\circ$ calculated with free wake model from NTUA, both with and without root vorticity

The figure shows results of the calculated axial velocity in the rotorplane of the Tjæreborg turbine (at 30%, 50% and 90% span). They are determined with a free wake code, developed by the National Technical University of Athens, NTUA, [12]. To distinguish the root vorticity effects, NTUA performed the calculations with two different models:

- The complete model (with identification 'with rv'). In this model the effect of the root vorticity is included automatically;
- A special version of the model (with identification 'without rv') in which root vorticity effects are excluded;

The calculations without root vorticity effects show the expected sinusoidal distribution, as induced by the tip vorticity. However the calculations, with root vorticity effects show qualitatively a surprisingly good agreement with the DUT measurements: Near the root a maximum at $\phi_r = 270$ degrees can be observed. At the tip a maximum at $\phi_r = 90$ degrees becomes apparent and the inflow distribution is very similar to the expected sinusoidal inflow distribution.

On basis of the available velocity measurements, an engineering model for the axial induced velocity could be developed and validated. The model consists of a second order Fourier series. The amplitudes and phases are fitted as function of radial position and yaw angle to the DUT measurements. The amplitudes are related to an azimuthal averaged induced velocity which is calculated from a standard blade element momentum calculation.

The new model led in many validation cases, to a considerable improvement in the prediction of the loads at yawed conditions compared to the previously used sinusoidal inflow model, although this was again based on indirect blade root moment measurements, where details on the radial dependency of the loading were lost. These details will become available from the present project.

It must be noted that the above given observations about the importance of skewed wake effects do not hold for low tip speed ratios. At these conditions the Dynamic Inflow projects showed that the advancing and retreating blade effect was dominant above the skewed wake effect. This is due to the fact that low tip speed ratios mean a larger value of V_{tang} compared to $\Omega \cdot r$. This enhances the advancing/retreating effect, see figure 2.1 (left). At the same time a low tip speed ratio can generally be associated with low induction which also makes the skewed wake effects less significant. Hence the inclusion of the skewed wake effects hardly effected the results at these conditions. At low tip speed ratios the axial blade loading was found to be maximum at vertical down position in a homogeneous ambient flow with positive yaw, due to the higher effective velocity, which apparently dominates the effect from the lower angle of attack at that position.

3. SELECTION OF CAMPAIGNS

In order to perform the study on yaw effects, it was attempted to find IEA Annex XVIII campaigns which fulfilled the following selection criteria:

1. The campaign should be taken at a substantial (mean) yaw angle (say > 15 degrees);
2. The averaged axial induction factor (which obviously only can be derived from calculations) should be ≥ 0.15 . At lower axial induction factors the loading variation over the rotor plane is mainly determined by the advancing and retreating blade effect;
3. The wind shear should be measured. This is an important requirement because the loading variation over the rotorplane interferes with the variation which is caused by wind shear and their effects are difficult to distinguish;
4. Preferably the yawed campaign should be compared with a similar campaign at (almost) zero yaw. The campaigns should be similar in terms of mean wind speed, pitch angle and rotor speed. Obviously the uncontrollable atmospheric conditions makes it very difficult to find campaigns which are fully comparable. Note that this condition is not strictly necessary since the yawing stability can be investigated without having a zero yaw campaign.

Then the only campaigns which satisfy these criteria have been measured on the ECN-facility.

3.1 Selected ECN campaigns

The selected campaigns are listed in table 3.1. The filenames are denoted through (n)y-rot-e-xxx, where 'ny' identifies a non-yawed campaign, 'y' identifies a yawed campaign and xxx is the sequence number. Furthermore, the table gives a rough estimate of the mean angle of attack at 80% span (α_{80}), the mean wind speed, the mean yaw angle, the pitch angle and the rotor speed. The wind shear (derived from the anemometer signals at hub height and at hub height $\pm R$) is also given. $shear_{up}$ gives the wind speed difference between the wind speed at hub height and the wind speed at hub height $+ R$ where $shear_{low}$ gives the difference between the wind speed at hub height and the wind speed at hub height $- R$. It is defined positive when the wind speed increases with height.

The yaw angles range from very positive to very negative yaw angles, with some moderate yaw angles in between. For every campaign a reference campaign is available at more or less zero yaw, which all have an axial induction factor above 0.15. Despite these high axial induction factors the angle of attack is still relatively large, (> 10 degrees) by which dynamic stall effects may play a role. The influence of dynamic stall effects is assessed in section 4.

file	$\overline{\alpha}_{80}$ deg	$\overline{V}_{\text{wind}}$ m/s	$\overline{\phi}_y$ deg	$\overline{\theta}_{\text{tip}}$ deg	$\overline{\Omega}$ rpm	$\overline{\text{shear}}_{\text{up}}$ [-]m	$\overline{\text{shear}}_{\text{low}}$ [-]
y-rot-e-001	11.84	9.46	42.9	-5.82	37.10	-0.03	1.36
ny-rot-e-005	19.44	10.97	0.9	-4.6	37.81	0.61	1.50
y-rot-e-002	17.95	8.40	39.8	-8.83	37.10	1.06	1.28
ny-rot-e-006	19.84	8.52	3.4	-7.0	37.0	0.76	0.21
y-rot-e-003	21.98	8.50	42.5	-11.83	36.67	0.63	1.53
ny-rot-e-007	25.35	9.71	2.6	-10.3	36.7	1.08	1.53
ny-rot-e-008	31.57	9.96	0.4	-12.6	36.3	0.79	0.84
y-rot-e-007	14.76	9.76	16.4	-5.82	37.60	0.36	1.31
ny-rot-e-006	19.84	8.52	3.4	-7.0	37.0	0.76	0.21
y-rot-e-008	22.89	8.18	14.2	-11.83	36.87	0.96	1.31
ny-rot-e-007	25.35	9.71	2.6	-10.3	36.7	1.08	1.53
y-rot-e-017	17.80	8.19	-30.0	-5.86	38.01	2.13	2.28
ny-rot-e-006	19.84	8.52	3.4	-7.0	37.0	0.76	0.21
y-rot-e-018	27.54	9.04	-34.0	-11.86	37.24	1.12	1.82
ny-rot-e-007	25.35	9.71	2.6	-10.3	36.7	1.08	1.53
y-rot-e-020	20.03	9.57	-49.2	-8.85	37.32	0.81	2.29
ny-rot-e-007	25.35	9.71	2.6	-10.3	36.7	1.08	1.53
y-rot-e-021	26.50	10.12	-49.2	-11.86	37.11	1.36	2.00
ny-rot-e-008	31.57	9.96	0.4	-12.6	36.3	0.79	0.84

Table 3.1 Global overview of selected ECN measurement campaigns at yawed and non-yawed conditions

Campaign nr.	a_{30} [-]	a_{60} [-]	a_{80} [-]	$C_{D,\text{ax}}$ [-]
ny-rot-e-005	0.197	0.179	0.176	0.457
ny-rot-e-006	0.301	0.299	0.272	0.685
ny-rot-e-007	0.251	0.208	0.217	0.557
ny-rot-e-008	0.233	0.180	0.190	0.500

Table 3.2 Calculated axial induction factors and $C_{D,\text{ax}}$ for ECN measurement files at non-yawed conditions

4. ANALYSIS OF RESULTS BY MEANS OF PHATAS CALCULATIONS

In this chapter, the results from the campaigns y-rot-e-001 and y-rot-e-002 (at positive yaw, $\phi_y = +42.9$ and $+39.8$ degrees, see table 3.1) and the results from the campaigns y-rot-e-017 and y-rot-e-021 (at negative yaw, $\phi_y = -30$ and -49.2 degrees) are discussed in detail. Thereto these campaigns are simulated with PHATAS-IV in which the engineering model, described in section 2, is implemented. The wind input to these PHATAS calculations was prescribed in the following way:

- The hub height wind speed from table 3.1 was prescribed; This wind speed was assumed to be constant;
- The bilinear wind shear from table 3.1 was prescribed ;
- The yaw angle from table 3.1 was prescribed. This yaw angle was assumed to be constant.

Then the local aerodynamic loads at different radial positions are binned as function of azimuth angle and a comparison is made between calculated and measured curves.

The figures 4.1 and 4.2 show the variation of the normal forces with azimuth angle for positive yaw (as a matter of fact the figure shows the values of $c_n \cdot V^2$, (with V the local velocity at the blade section) which differ from the actual normal force by the constant $0.5 \rho c$). These results are very representative for the other results at positive yaw angles (although this is less true for the smaller positive yaw angles). In the figures 4.3 and 4.4 the results of the 'normal forces' are presented as function of azimuth angle for the negative yaw angles. These results are very representative for negative yaw angles. The corresponding results at zero yaw are also presented.

It must be noted that the axial (out of plane) loads which determine the yawing stability are not solely a result of the aerodynamic normal forces. The aerodynamic tangential force along the chord force will, because of the twist and pitch angle, also contribute to the out of plane direction, but this contribution is very small, in particular for the present campaigns which are taken at a negative pitch angle.

The complete comparison (not only on basis of normal forces but also on dimensionless c_n values and inflow velocities) can be found in Appendix A.

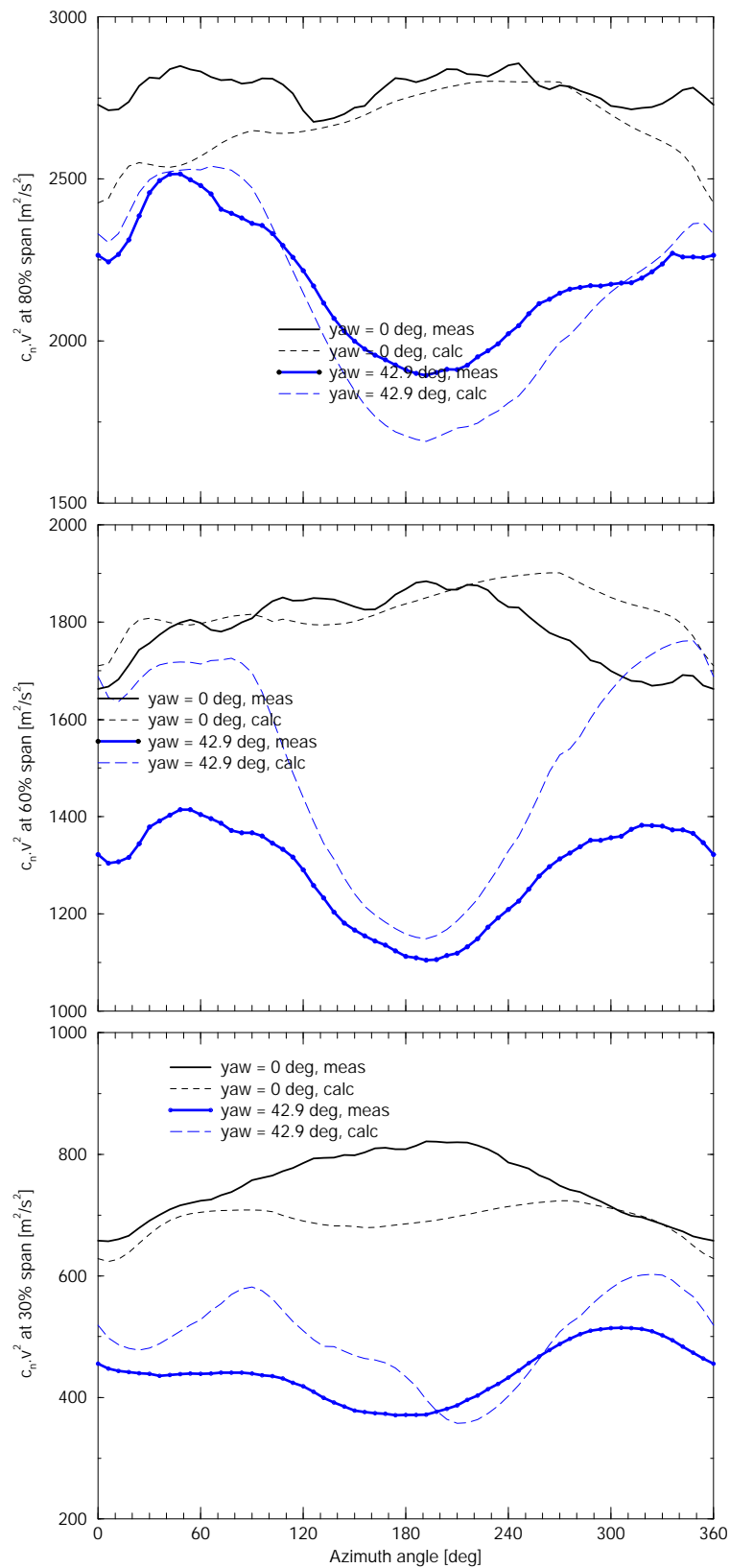


Figure 4.1 ECN campaign y-rot-e-001: $n - \phi_r$ at $\phi_y = 42.9$ deg and at $a \approx 0.2$; 80% span (top), 60% span, 30% span (bottom)

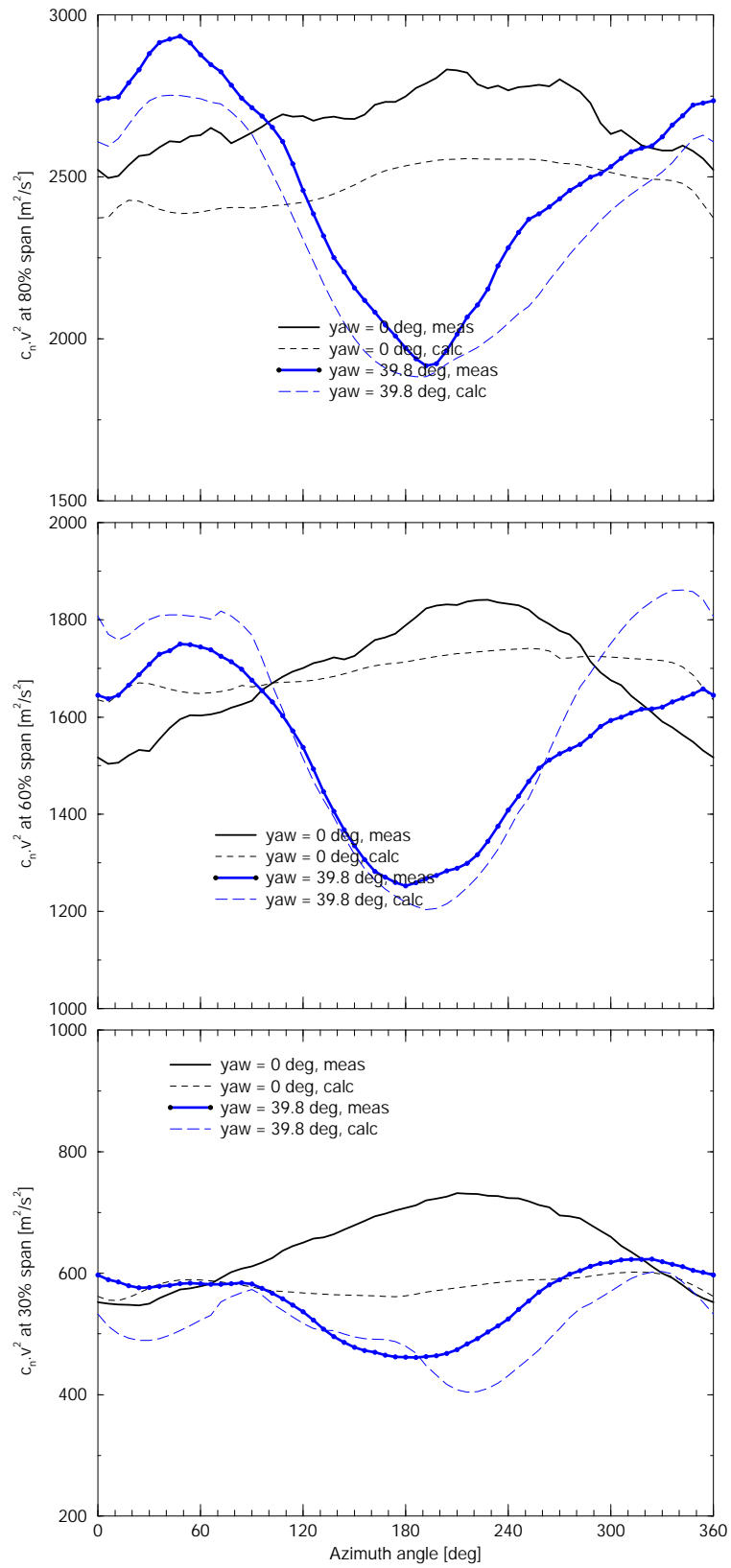


Figure 4.2 ECN campaign *y-rot-e-002*: $n - \phi_x$ at $\phi_y = 39.8$ deg and at $a \approx 0.3$; 80% span (top), 60% span, 30% span (bottom)

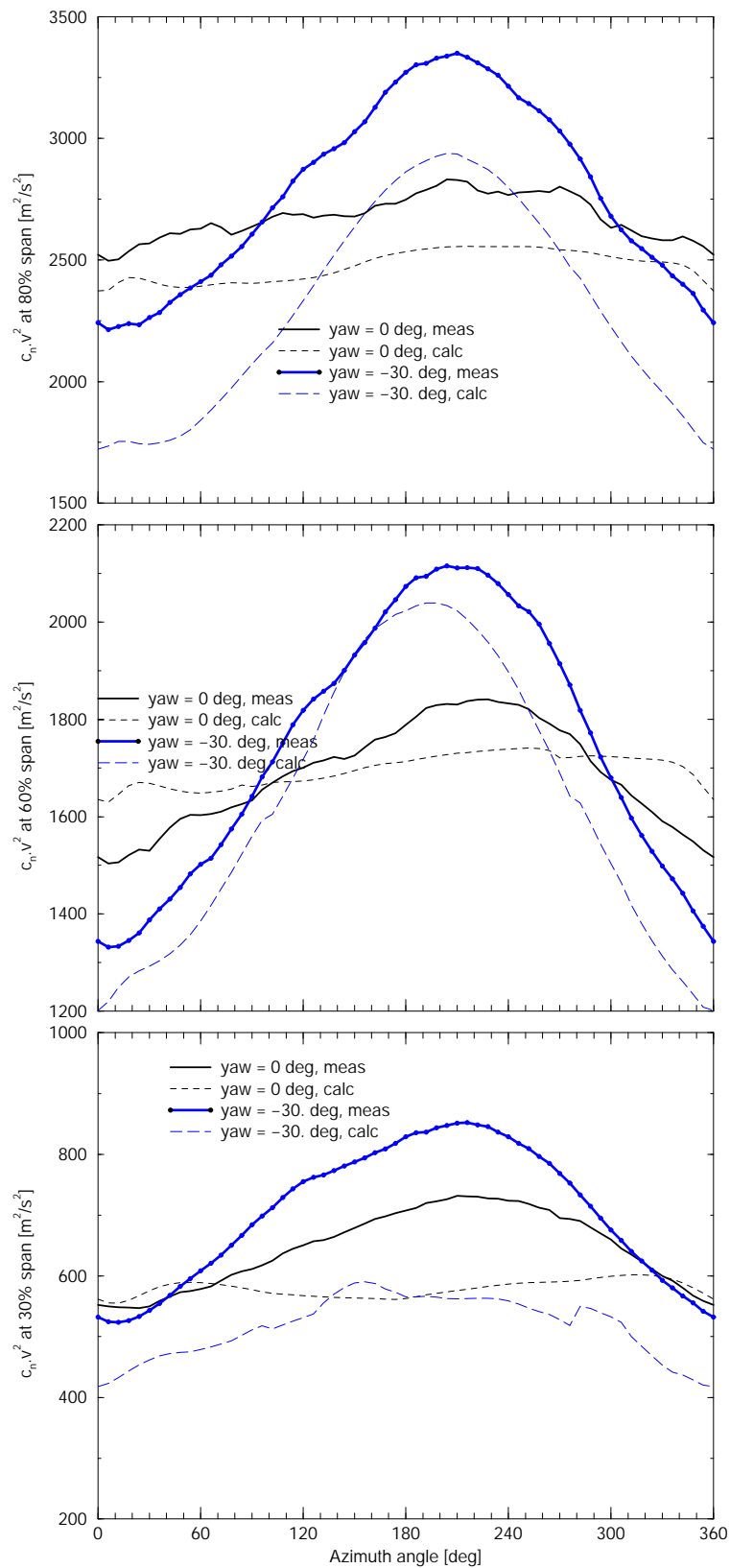


Figure 4.3 ECN campaign y-rot-e-017: $n - \phi_r$ at $\phi_y = -30$ deg. and at $a \approx 0.3$; 80% span (top), 60% span, 30% span (bottom)

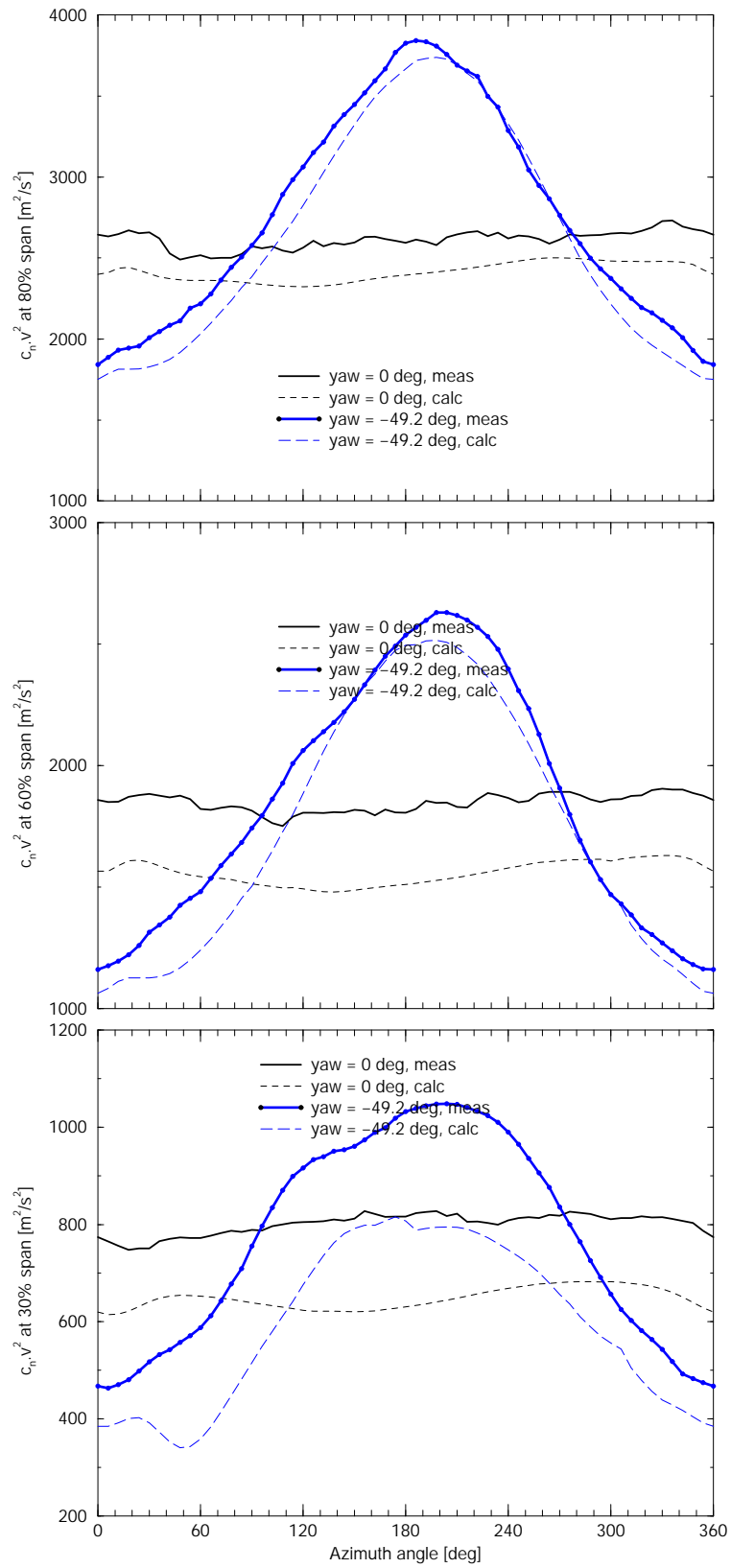


Figure 4.4 ECN campaign *y-rot-e-021*: $n - \phi_x$ at $\phi_y = -49$ deg. and at $a \approx 0.2$; 80% span (top), 60% span, 30% span (bottom)

The following comments can be made:

- Generally speaking the shape of the $n - \phi_r$ curve at yawed conditions is predicted very well with the engineering model from PHATAS, but this is less true at the 60% section, where some cases show a large overprediction of normal forces near the 0 degrees azimuth for unknown reasons. It should also be mentioned that already at zero yaw, the calculated normal forces differ from the measured values. These differences will, most likely, also be reflected in the prediction of the much more difficult yawed conditions;
- As expected the variation of the normal forces with ϕ_r (i.e. the amplitude of $n - \phi_r$) increases with increasing yaw angles. This is true in both calculations and measurements, in particular at the 80% section;
- The most interesting observation can be found for the positive yaw campaigns, see the figures 4.1 and 4.2:
 - At 80% span, the maximum in normal force is found in the upwind side of the rotorplane (near $\phi_r \approx 50$ degrees). As such the tip section yields a stabilizing yawing moment contribution as expected from the discussion in section 2. At this spanwise location, there is a good agreement between measurements and PHATAS calculational results;
 - At 30% span, the maximum in normal force is found at the downwind side of the rotorplane (near $\phi_r \approx 300$ degrees). As such the root section does contribute to a destabilizing yawing moment indeed! As for the 80% section, there is a very reasonable agreement between calculated and measured variation and a destabilizing yawing moment contribution is found both calculations and measurements;
 - From the discussion in section 2, the maximum force from the induced velocity distribution at the tip would be expected to occur at precisely $\phi_r = 90$ degrees where it is supposed to be at precisely 270 degrees near the very root. However the following effects disturb this 'idealised' picture.
 - * The 30% and the 80% span are close, but not fully at the root and the tip section. In figure 4.5 the calculated induced velocities are given. It is found that the minimum induced velocity at 30% span occurs at $\phi_r \approx 230$ degrees and the minimum induced velocity at 80% span occurs at $\phi_r \approx 105$ degrees;
 - * The load variation does not straightforwardly follow the induced velocity variation but it is also determined by the following effects:
 - The advancing and retreating blade effect. At positive yaw, this makes the maximum loading to appear at 0 degrees and the minimum loading at 180 degrees. The effect is most notable near the root sections;
 - The wind shear. This makes the maximum loading at $\phi_r = 180$ degrees and the minimum loading at $\phi_r = 0$ degrees. As such it opposes the advancing and retreating blades at positive yaw, where it enhances the advancing and retreating blade effect at negative yaw. The effects from windshear will be most notable near the tip section;
 - The structural flexibility;
 - The tower shadow;
 - The cone and tilt angle;
 - The effect from dynamic stall;

The importance of these additional effects can be assessed from figure 4.6. This figure shows (by means of calculations) the sensitivity of the normal force variation to the combination of these additional effects (flexibilities, wind shear, dynamic stall, tower shadow and tilt and cone angle). Although these are theoretical results, the generally good agreement between calculations and measurements gives some confidence in the validity of it. The sum of all additional effects turns out to have a rather large influence on the results (in particular at the 30% section). Nevertheless the main conclusion remains: With and without additional effects, the yawing moment contribution is destabilizing at the 30% section (the maximum normal force is at the downwind side of the rotorplane) and stabilizing at the 80% section. As a matter of fact, the neglect of additional effects makes the destabilizing yawing moment contribution at the 30% span even stronger because it yields generally speaking higher normal forces at the downwind side and lower normal forces on the upwind side. Vice versa, the inclusion of additional effects tend to stabilize the yawing moment at 30% span. Some further sensitivity studies showed that this is mainly caused by the stabilizing effects from the cone angle, flexibilities and dynamic stall. At the 80% section the neglect of the additional effects tends to neutralize the (stabilizing) yawing moment contribution and vice versa, the inclusion of additional effects tends to stabilize the yawing moment at 80% span. This is mainly caused by the effect of wind shear: At positive yaw, the wind shear compensates the neutralizing advancing and retreating blade effect.

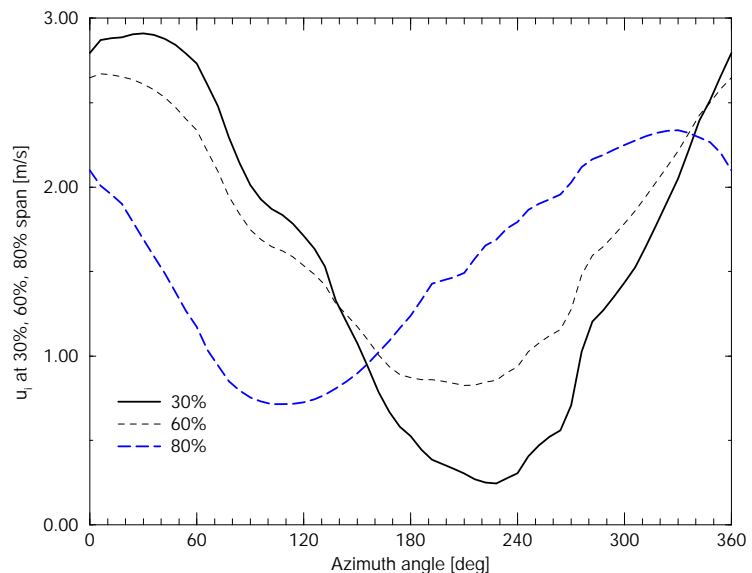


Figure 4.5 *ECN campaign y-rot-e-001: Calculated $u_i - \phi_r$ at $\phi_y = +42$ deg. and at a ≈ 0.2 ; 80% span (top), 30% span (bottom)*

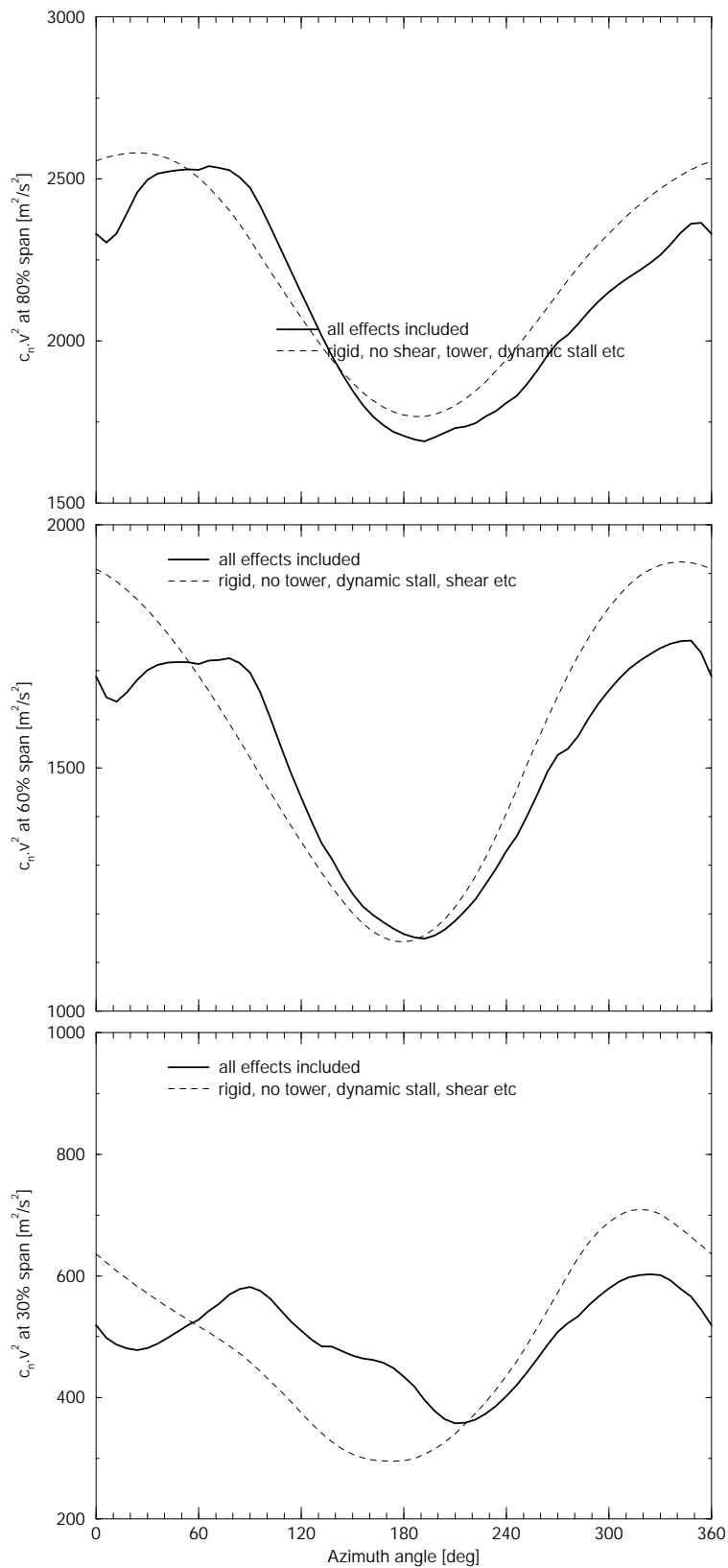


Figure 4.6 ECN campaign y-rot-e-001: Calculated $n - \phi_r$ at $\phi_y = +42$ deg. and at $a \approx 0.2$, with and without additional effects; 80% span (top), 30% span (bottom)

- At first sight it would be expected that the results at negative yaw could be found from the distribution at positive yaw by 'mirroring' around the 0-180 degrees azimuth axis. Hence the maximum normal force at the tip would be expected to be close to $\phi_r = 270$ degrees where the maximum at the root is expected to be close to $\phi_r = 90$ degrees. Comparison of the figures 4.2 and 4.1 with the figures 4.4 and 4.3 shows that this is not the case:
 - At negative yaw, the maximum loading is found near $\phi_r = 180$ degrees (actually slightly above 180 degrees) and the minimum loading is found near $\phi_r = 0$ degrees. This corresponds to a neutral yawing moment contribution, very well in line with the predictions from the PHATAS code;
 - A deviation occurs at the 30% section in figure 4.3: The measured yawing moment contribution is stabilizing where the calculations indicate a destabilizing yawing moment contribution. It must be noted that a similar discrepancy is already found at the zero yaw campaign. Furthermore the measured wind shear for case y-rot-e-017 is extremely large (more than 25% over both the upper and lower part of the rotor plane) which puts some doubt on the representativeness of this result.

Now it must be noted that the conditions for the negative yaw cases are close but still not sufficiently comparable to the conditions for the positive yaw cases: At the negative yaw cases the axial induction factor is relatively low or the wind shear is very strong. Both effects tend to stabilize the yawing moment. If the wind speed for the negative yaw cases would have been lower, it is expected that the same conclusions could be drawn as for the positive yaw cases: Calculations at negative yaw, at a lower wind speed ($V=7.12$ instead of $V=10.12$ m/s) show much more pronounced effects of the induced velocity distribution, see figure 4.8: A destabilizing yawing moment contribution is found at 30% span and a stabilizing yawing moment contribution at 80% span. Furthermore, it is found by means of calculations that without additional effects (i.e. without structural flexibility, dynamic stall, wind shear etc) the load distributions at positive yaw is the precise mirror of the load distribution at negative yaw. Hence a possibly asymmetry between positive and negative yaw is caused by the additional effects. The sensitivity to the additional effects at negative yaw can be found in figure 4.7.

- The neglect of additional effects (flexibilities, dynamic stall, tower, tilt) yields a stronger destabilizing yawing moment contribution at the 30% section similar to the situation at positive yaw angle and vice versa it can be concluded that the additional effects stabilize the yawing moment contribution. Further sensitivity studies showed that this is mainly a result from the dynamic stall effects and to a smaller extent from the cone angle.
- The neglect of additional effects at the 80% section has a limited influence but it tends to destabilize the yawing moment contribution. Vice-versa it can be concluded that the inclusion of the additional effects tend to stabilize the yawing moment. Sensitivity studies showed that the wind shear is having a slight destabilizing effect (as explained above), but this is compensated by a slightly stabilizing contribution from all other effects.

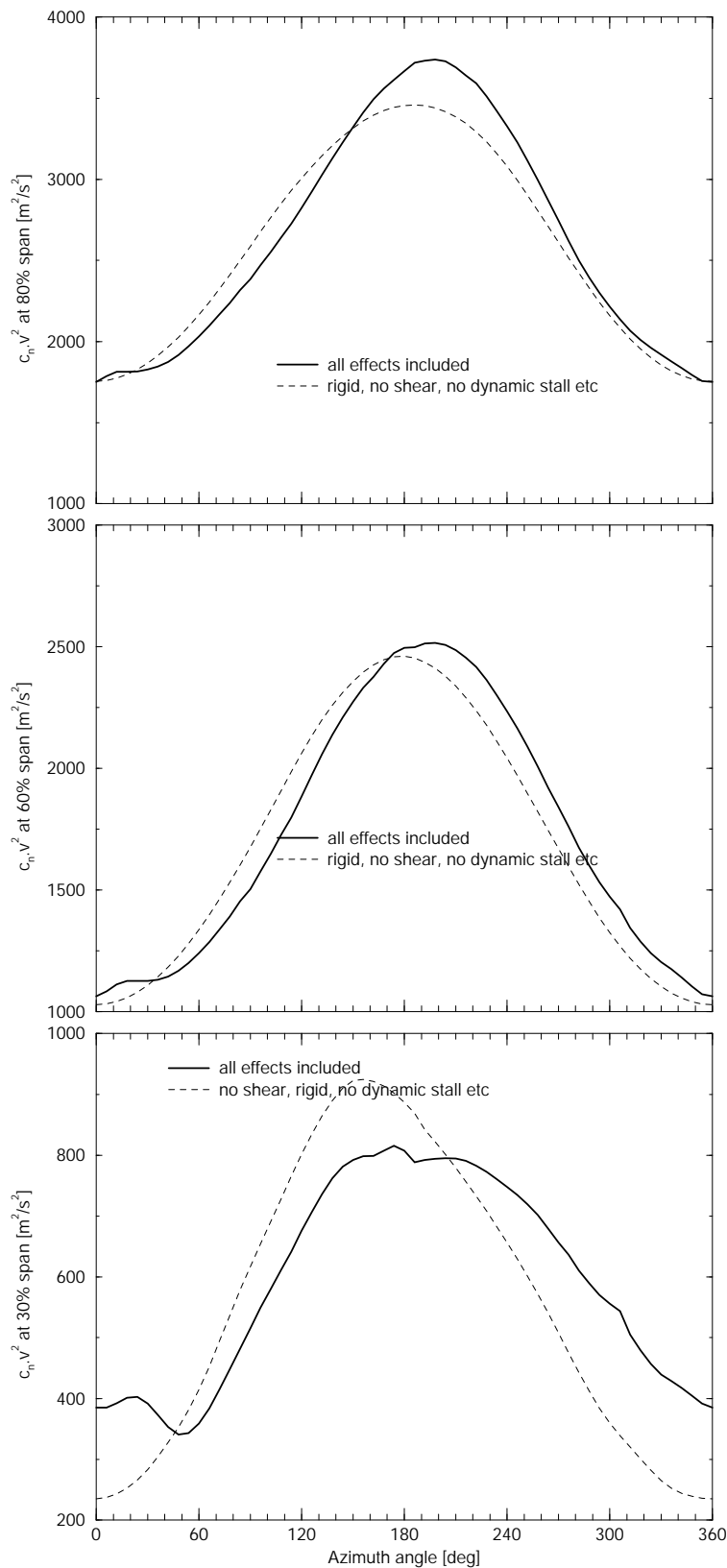


Figure 4.7 Calculated $n - \phi_r$ at $\phi_y = -49$ deg. and at $a \approx 0.2$, with and without additional effects; 80% span (top), 30% span (bottom)

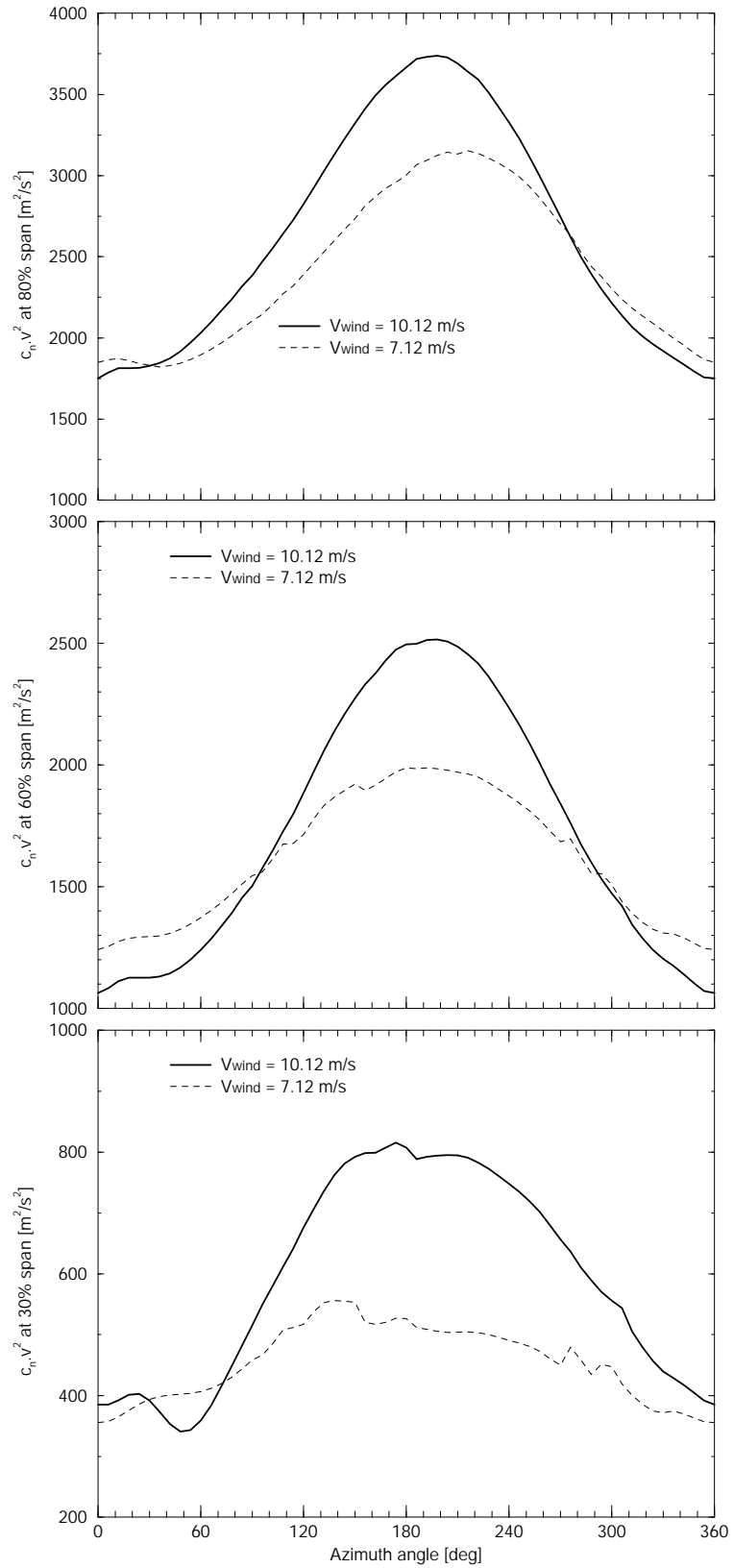


Figure 4.8 Calculated $n - \phi_r$ at $\phi_y = -49$ deg. at $V_{wind} = 10.12$ m/s and $V_{wind} = 7.12$ m/s; 80% span (top), 30% span (bottom)

5. AWSM CALCULATIONS

Campaign y-rot-e-001 (i.e. the campaign at a yaw angle of 42.9 degrees, see table 3.1) has been simulated with the AWSM code. AWSM is a newly developed free wake lifting line model which automatically models the effects from the skewed wake geometry on the inflow velocity distribution. The code is described in [10].

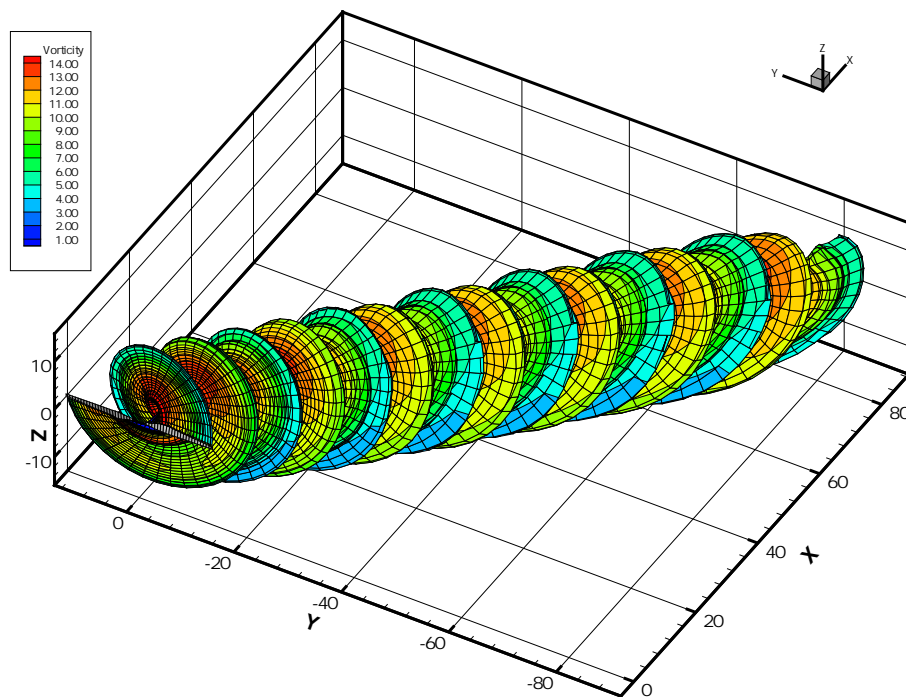


Figure 5.1 *Wake geometry calculated by AWSM*

The results of the normal force distribution at 30% and 80% span are presented in figure 5.2. The result obtained with the PHATAS code is also given. The corresponding wake geometry is presented in figure 5.1. It can be observed that the AWSM results differ considerably at the 30% section, where the agreement at the 80% section is very well. Part of the deviation at 30% span can be caused by dynamic stall effects. These effects are not taken into account in the AWSM model, where they do have some influence, at least according to the sensitivity study which has been performed with PHATAS, see section 4.

Within IEA Annex XX, i.e. the analysis of the NREL measurements on a 10 m diameter turbine in the NASA-Ames wind tunnel, a more thorough validation of the AWSM code will be performed, which hopefully sheds some light on the present puzzling results.

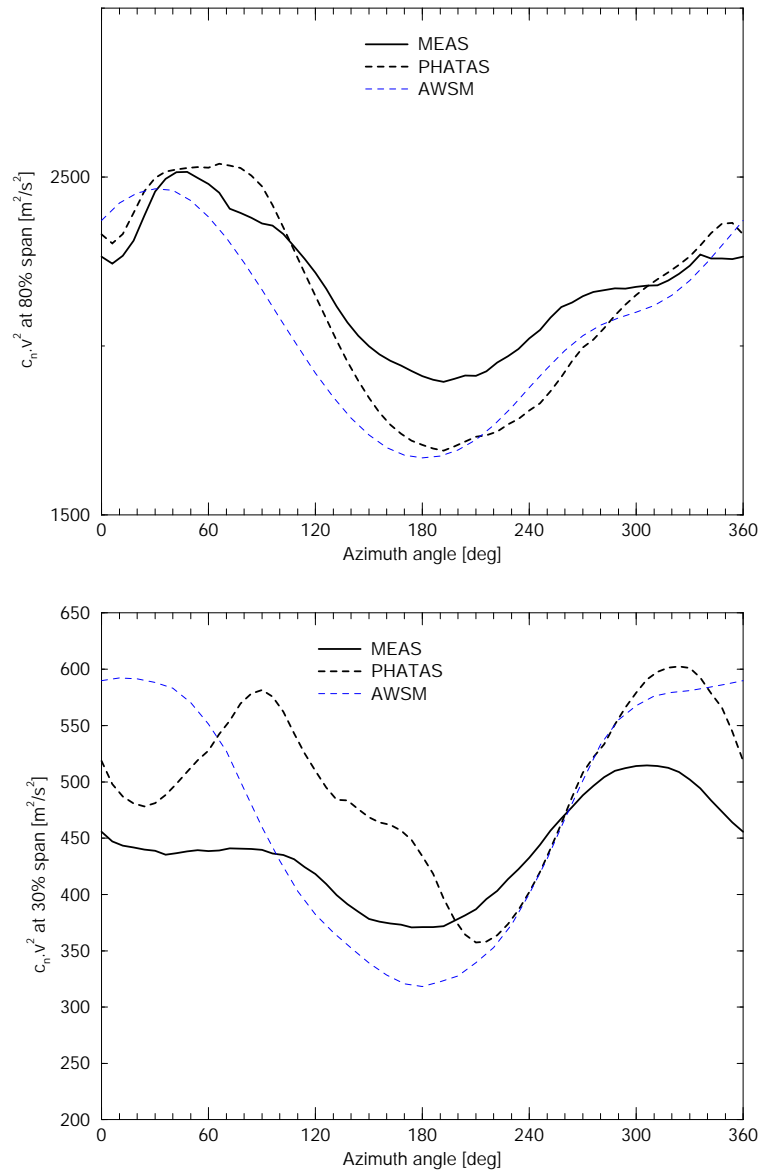


Figure 5.2 ECN campaign y-rot-e-001: $n - \phi_r$ at $\phi_y = 42.9$ deg. and at $a \approx 0.2$; 80% span (top), 30% span (bottom); Calculated with PHATAS and AWSM

6. CONCLUSIONS

The most important conclusion from the present study is, that local aerodynamic measurements along a wind turbine blade show a destabilizing yawing moment contribution to be possible at the root of a blade, where at the same time the tip can contribute to a stabilizing yawing moment. The destabilizing effect at the root can slightly be reduced by structural flexibility, dynamic stall, cone angle etc.

Generally speaking the PHATAS code predicts the shape of the aerodynamic normal force as function of azimuth angle (and as such the yawing stability) well and better than the result expected from a conventional Glauert type of model. Most important is that PHATAS predicts the destabilizing yawing moment contribution at the root where at the same time the tip is predicted to contribute a stabilizing yawing moment. First results from the new free wake code AWSM are promising but have also led to some unanswered questions.

REFERENCES

- [1] H. Snel and J.G Schepers (ed.) . “JOULE1: Joint investigation of Dynamic Inflow Effects and Implementation of an Engineering Method”. ECN-C-94-107, December 1994.
- [2] J.G. Schepers and H. Snel (ed.) . “JOULE2: Dynamic Inflow: Yawed Conditions and Partial Span Pitch”. ECN-C-95-056, June 1995.
- [3] J.G Schepers et al. “Final report of IEA Annex XVIII’ Enhanced Field Rotor Aerodynamics Database”. ECN-C-02-016, February 2002.
- [4] J.G. Schepers, R. van Rooij and A. Bruining . “Detailed aerodynamic measurements: Analysis of results ”. In *Proceedings of European Wind Energy Conference, EWEC*, Madrid, June 2003.
- [5] R. van Rooij A. Bruining and J.G. Schepers. “Validation of some rotor stall models by analysis of the IEA Annex XVIII field data ”. In *Proceedings of European Wind Energy Conference, EWEC*, Madrid, June 2003.
- [6] J.G. Schepers, L. Feigl, R. van Rooij and A. Bruining. “Validation of aero-elastic codes, using detailed aerodynamic measurements ”. In *Proceedings of EAWE, conference, 'The Science of Making Torque from the Wind'*, Delft, April 2004.
- [7] J.G. Schepers, L. Feigl, R. van Rooij and A. Bruining. “Analysis of detailed aerodynamic measurements, using results from an aero-elastic code ”. In *Submitted to Wind Energy Journal*, August 2004.
- [8] J.G. Schepers . “An engineering model for yawed conditions developed on basis of wind turnnel measurements”. In *ASME Wind Energy Symposium, Reno USA*, January 1999.
- [9] A. Björck. “Dynamic Stall and Three Dimensional Effect ”. FFA-TN –1995-31, FFA, 1995.
- [10] A. van Garrel. “Development of a wind turbine aerodynamics simulation module ”. ECN-C –03-079, ECN, August 2003.
- [11] Glauert, H. *A general theory for the Autogyro*. ARC R - M 1111, November 1926.
- [12] S. Voutsinas , M. Belessis and S. Huberson. “Dynamic inflow effects and vortex particle methods”. In *Proceedings ECWEC conference, Travemunde, 8-12 March 1993*, page 428, March 1993.

APPENDIX A. AZIMUTHALLY BINNED AVERAGED VALUES ON ECN TURBINE

It is recalled that the azimuth angle ϕ_r is defined such that $\phi_r = 0$ degrees means that the blade is pointing down in vertical position (i.e. 6 o'clock position), where the yaw angle is defined positive according to fig. A.1. Hence for positive yaw, the upwind side of the rotorplane is between 0 and 180 degrees azimuth and for negative yaw it is between 180 and 360 degrees azimuth.

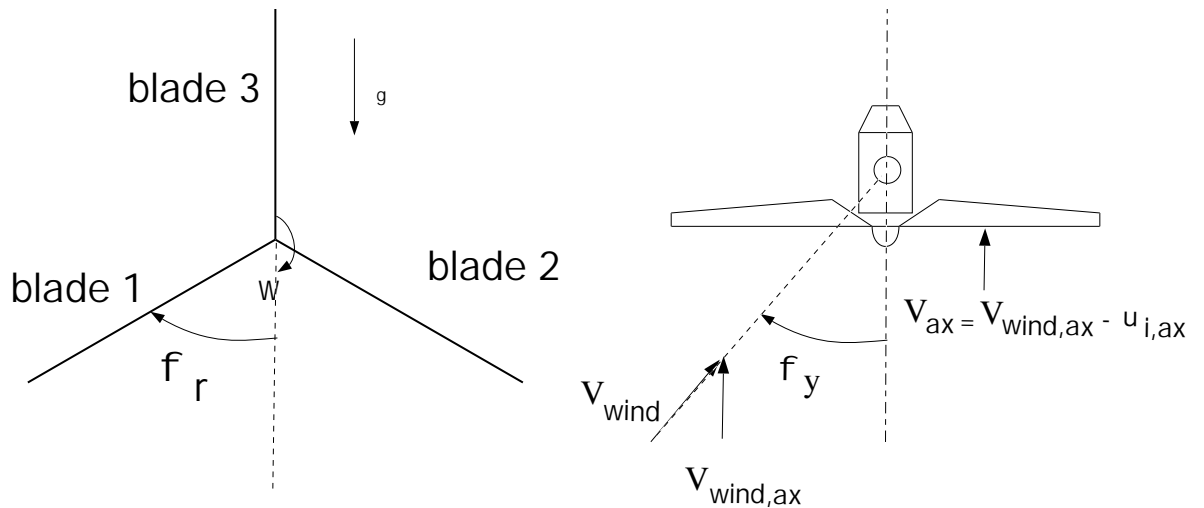


Figure A.1 *Definition of axial induced velocity, yaw angle and azimuth angle*

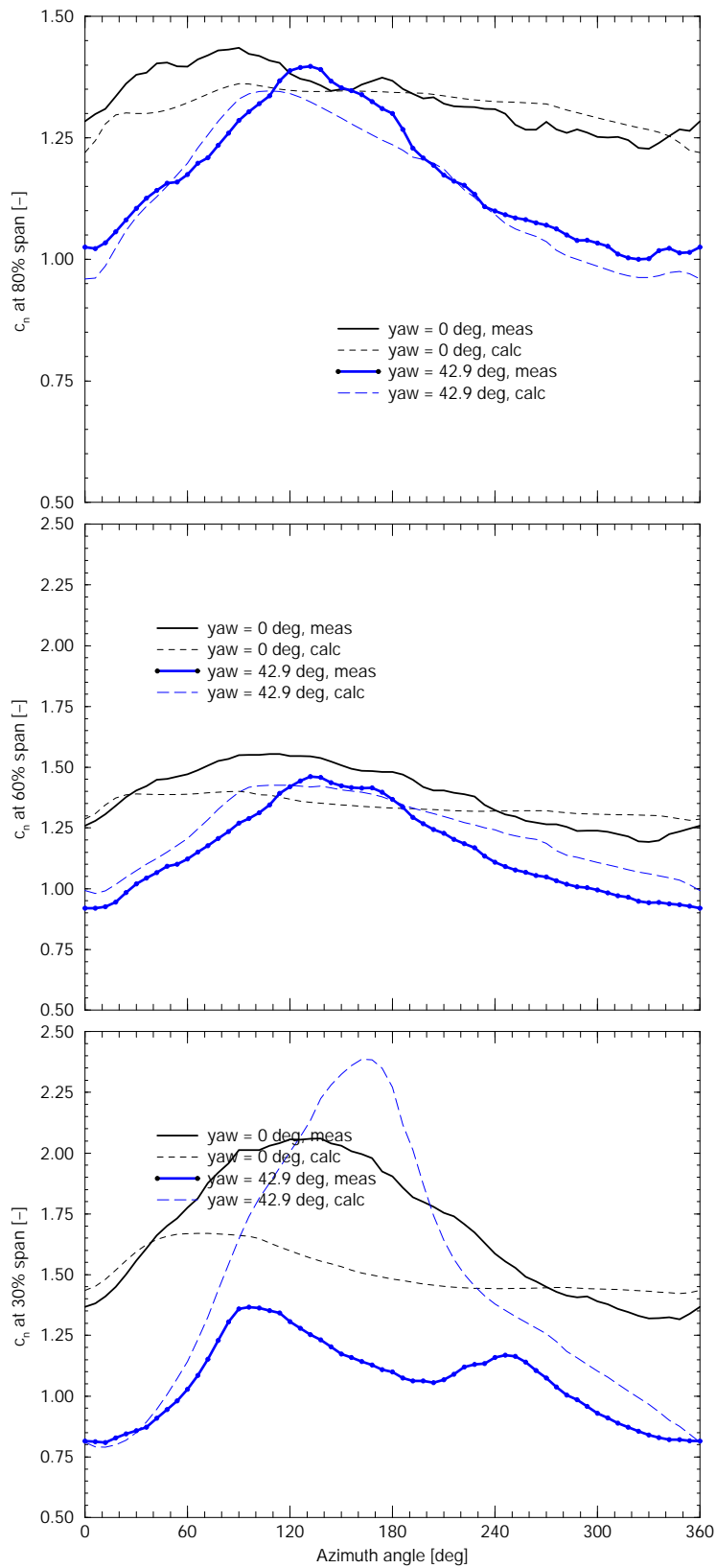


Figure A.2 ECN measurements: $c_n - \phi_r$ at $\phi_y = 42.9$ deg. and at $a \approx 0.18$; 80% span (top), 60% span, 30% span (bottom)

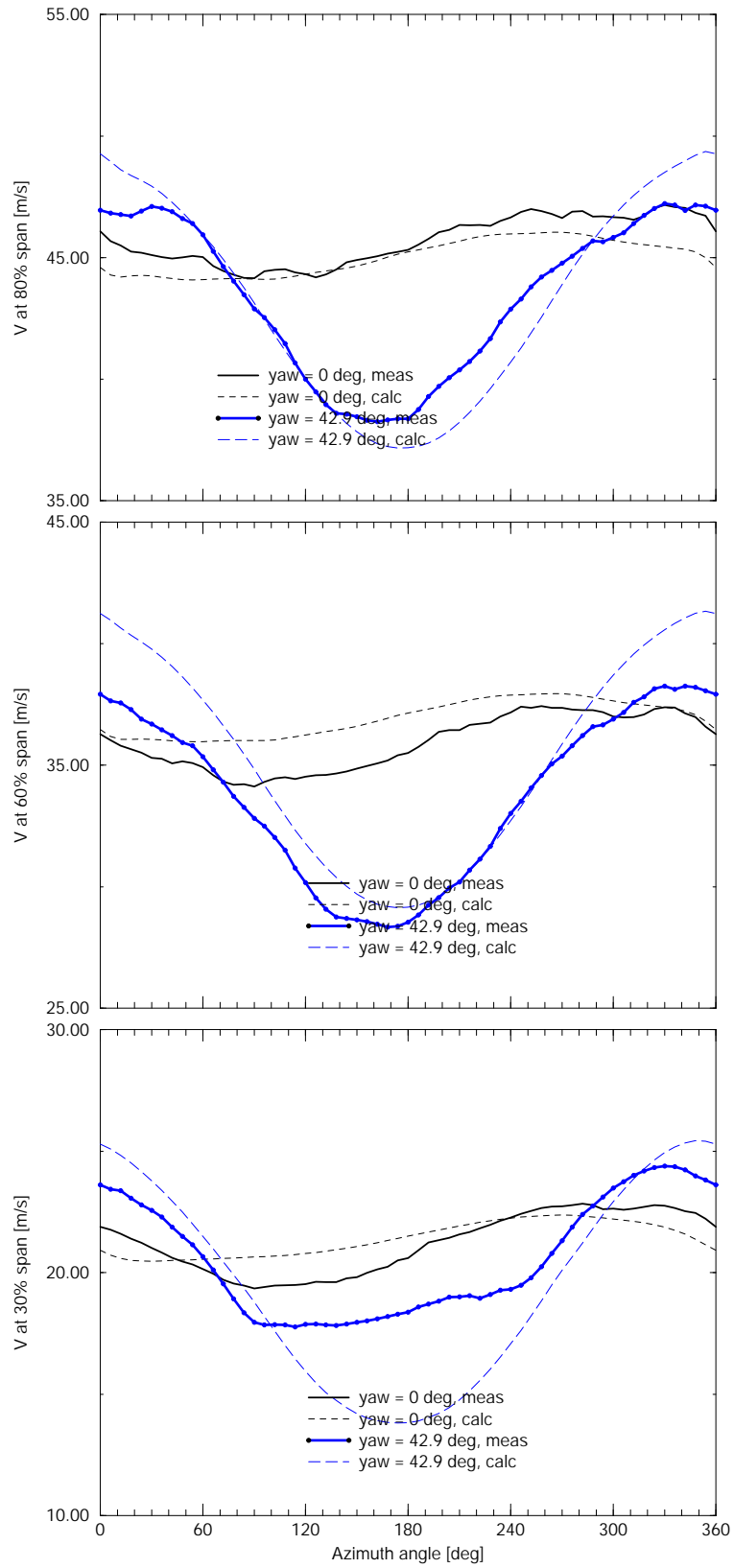


Figure A.3 ECN measurements: $V - \phi_r$ at $\phi_y = 42.9$ deg. and at $a \approx 0.18$; 80% span (top), 60% span, 30% span (bottom)

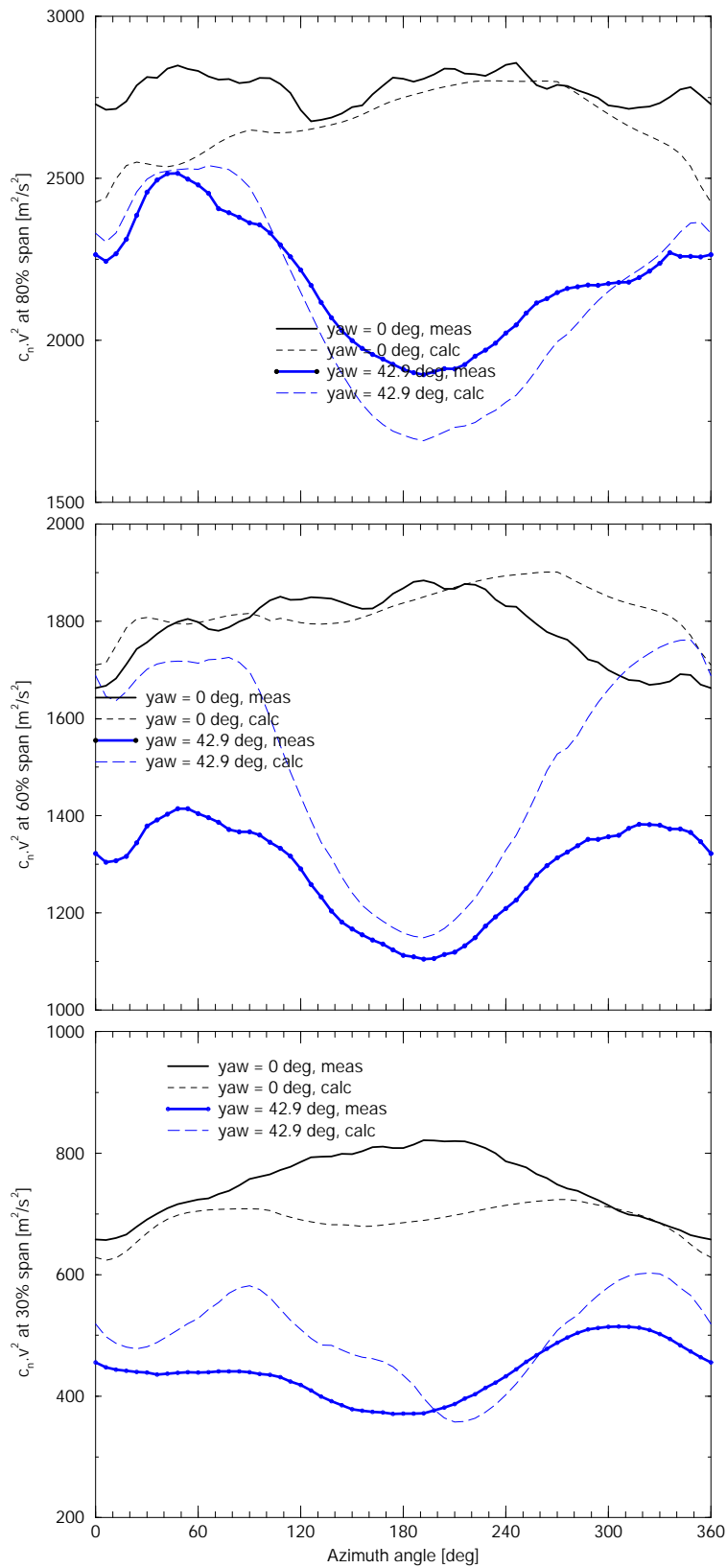


Figure A.4 ECN measurements: $n - \phi_r$ at $\phi_y = 42.9$ deg. and at $a \approx 0.18$; 80% span (top), 60% span, 30% span (bottom)

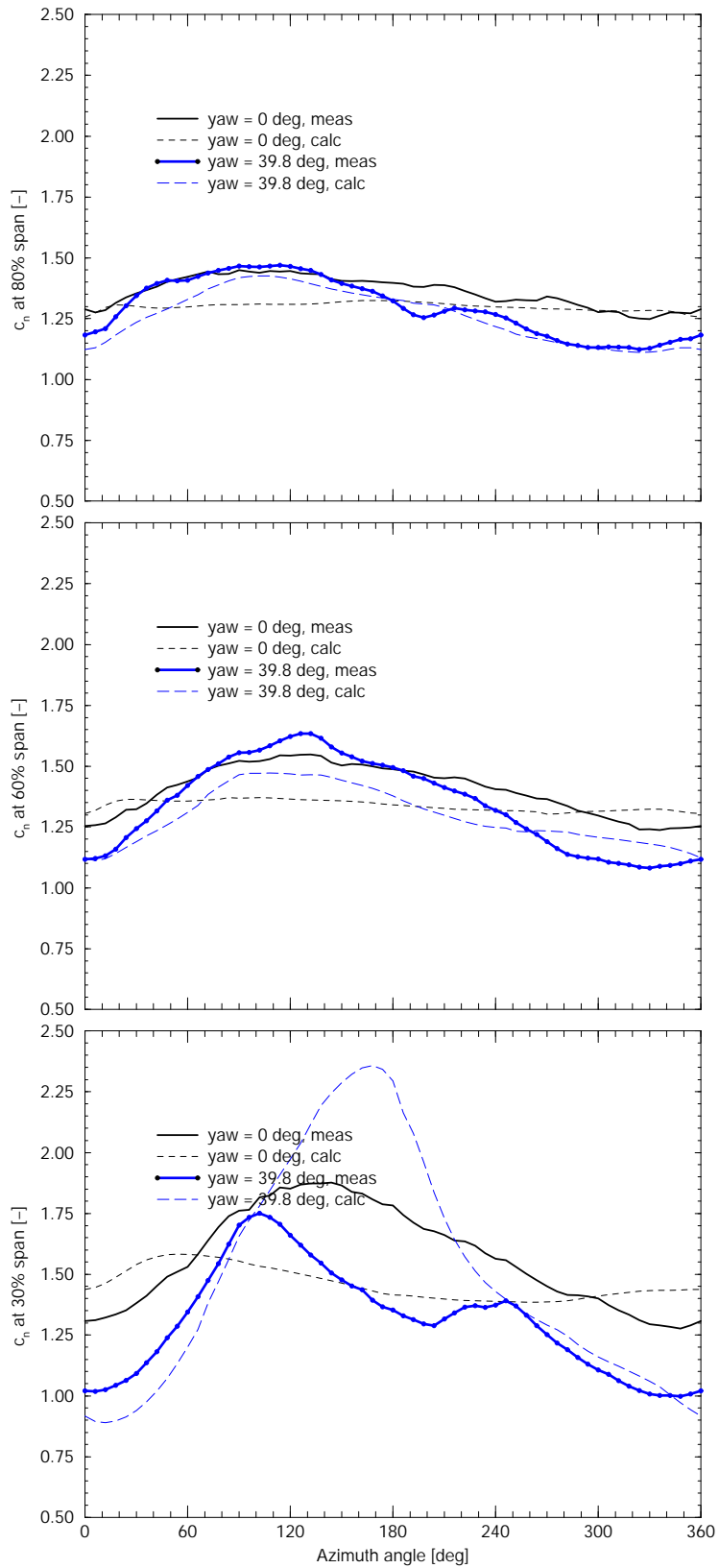


Figure A.5 ECN measurements: $c_n - \phi_r$ at $\phi_y = 39.8$ deg. and at $a \approx 0.3$; 80% span (top), 60% span, 30% span (bottom)

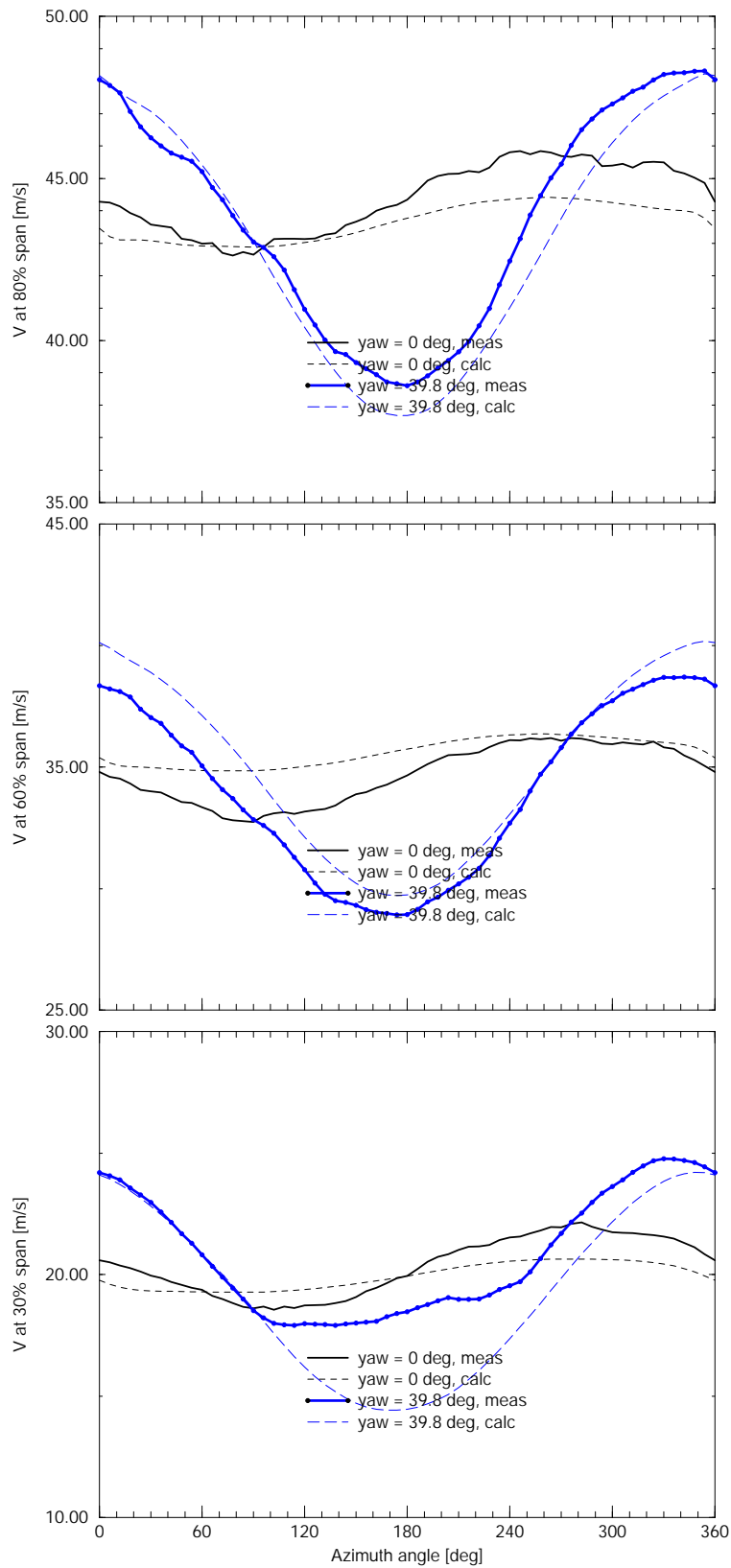


Figure A.6 ECN measurements: $V - \phi_r$ at $\phi_y = 39.8$ deg. and at $a \approx 0.3$; 80% span (top), 60% span, 30% span (bottom)

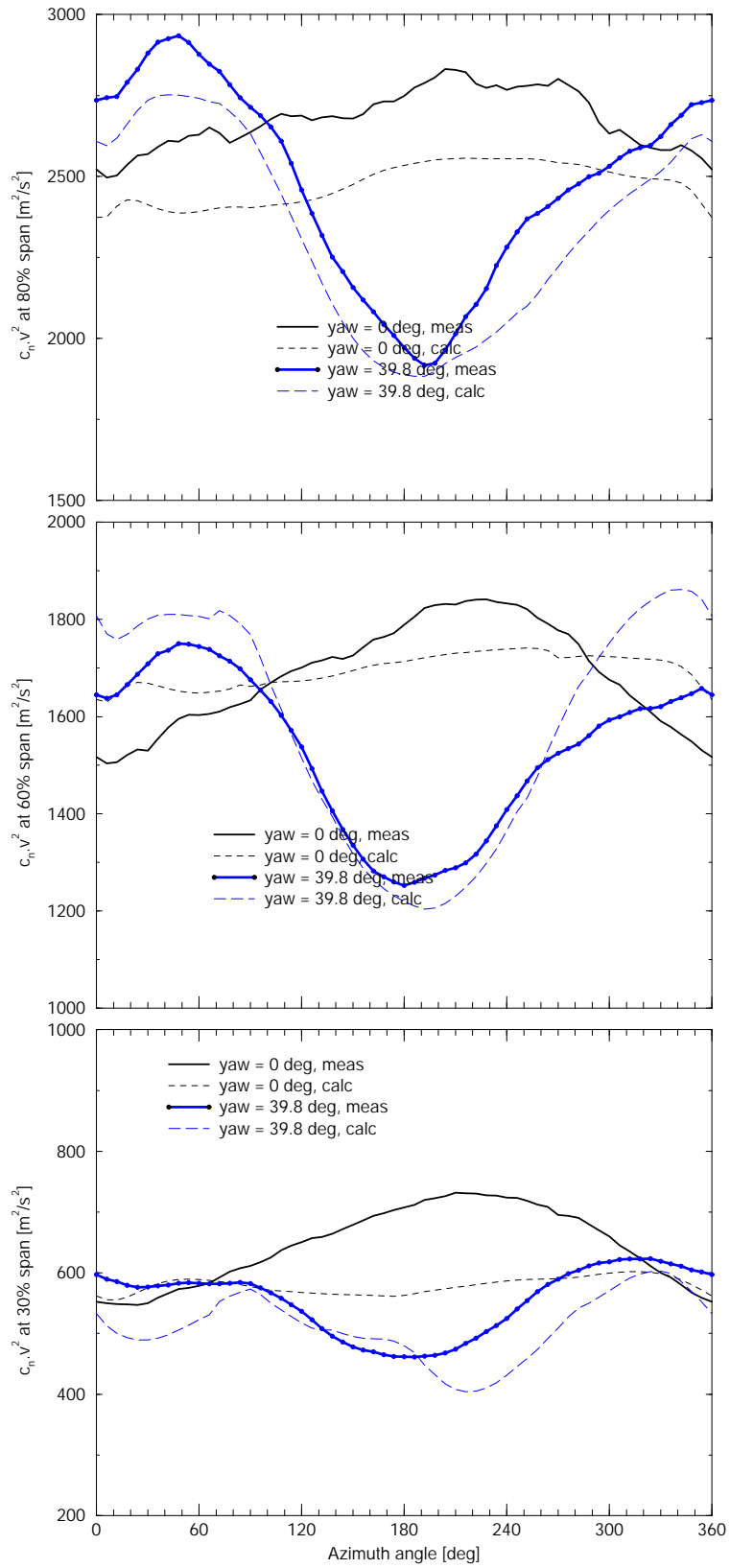


Figure A.7 ECN measurements: $n - \phi_r$ at $\phi_y = 39.8$ deg. and at $a \approx 0.3$; 80% span (top), 60% span, 30% span (bottom)

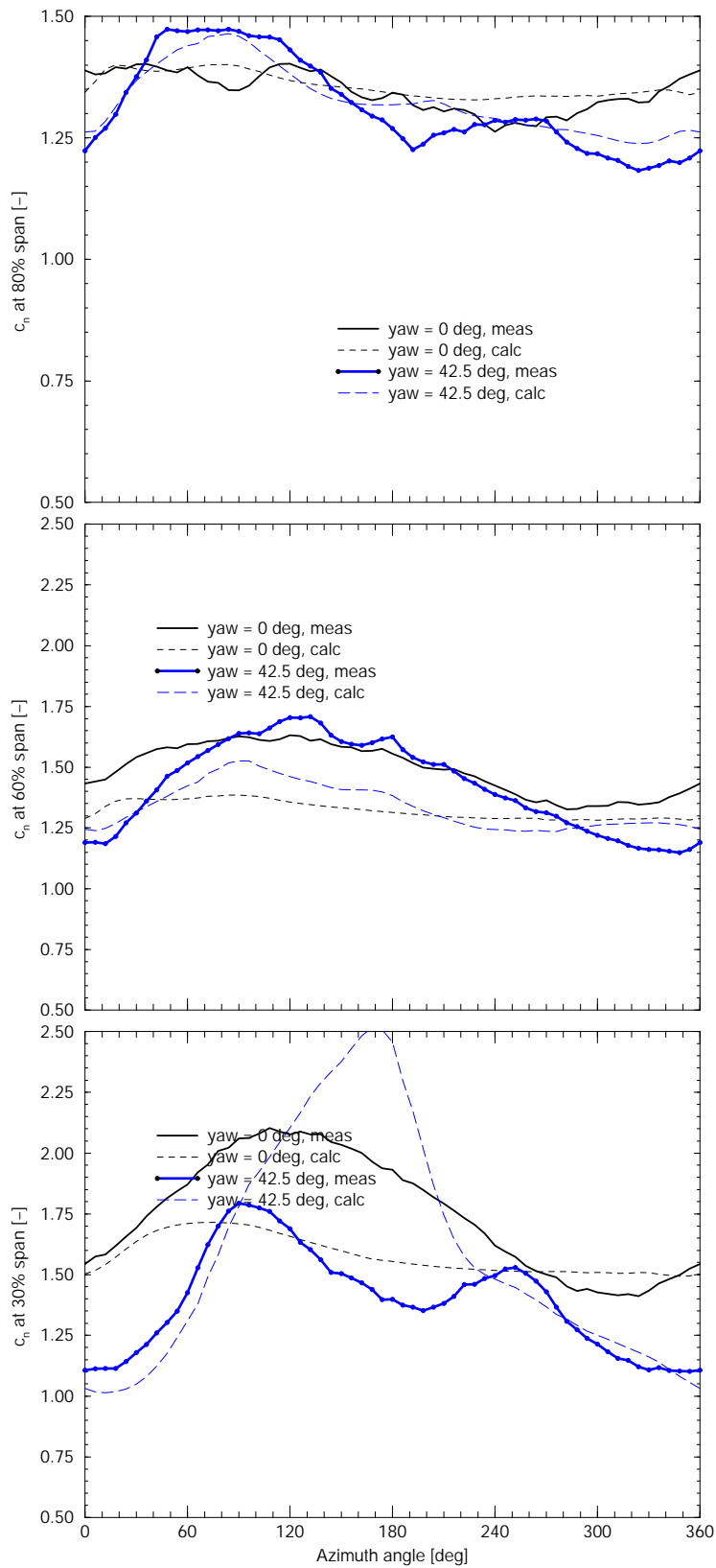


Figure A.8 ECN measurements: $c_n - \phi_r$ at $\phi_y = 42.5$ deg. and at $a \approx 0.2$; 80% span (top), 60% span, 30% span (bottom)

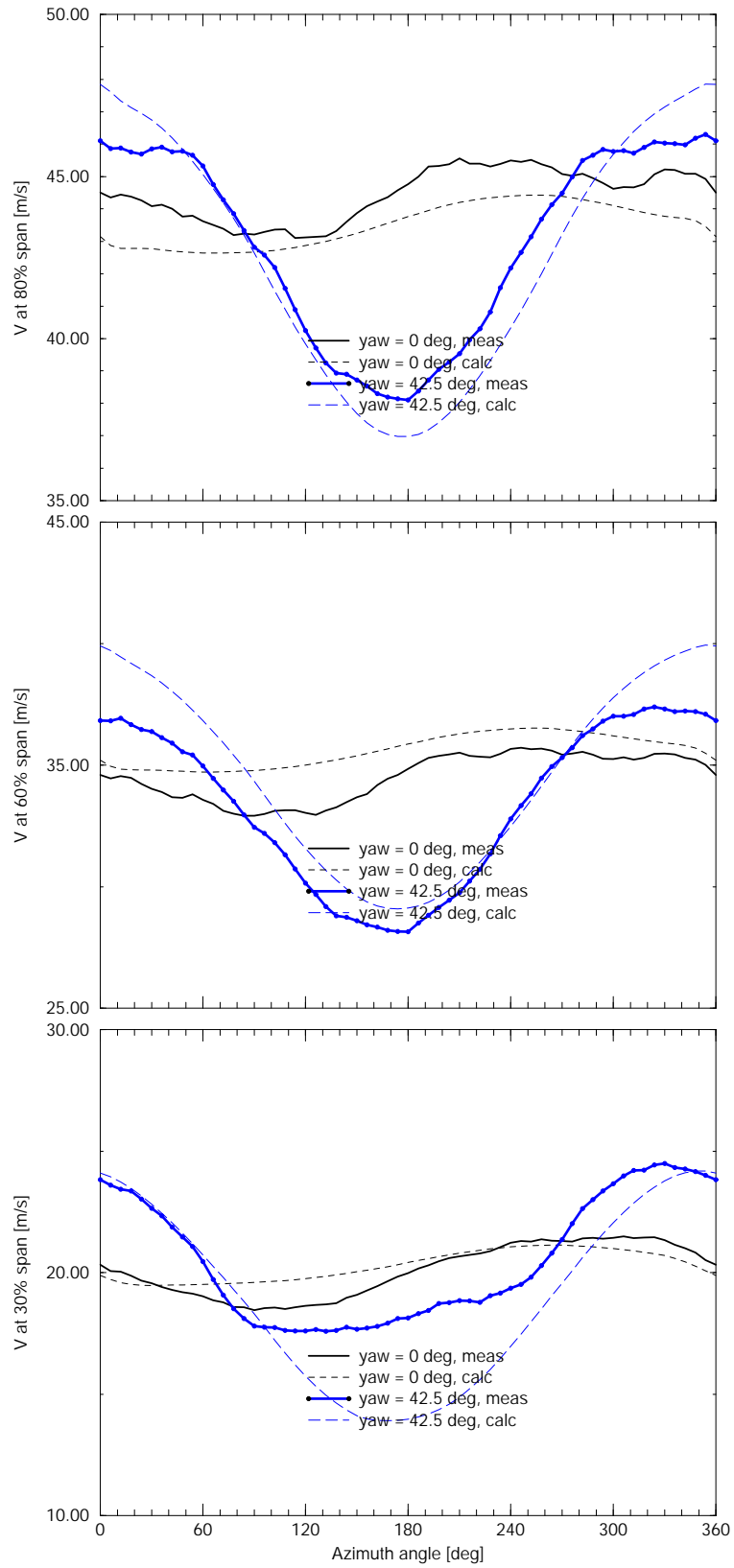


Figure A.9 ECN measurements: $V - \phi_r$ at $\phi_y = 42.5$ deg. and at $a \approx 0.2$; 80% span (top), 60% span, 30% span (bottom)

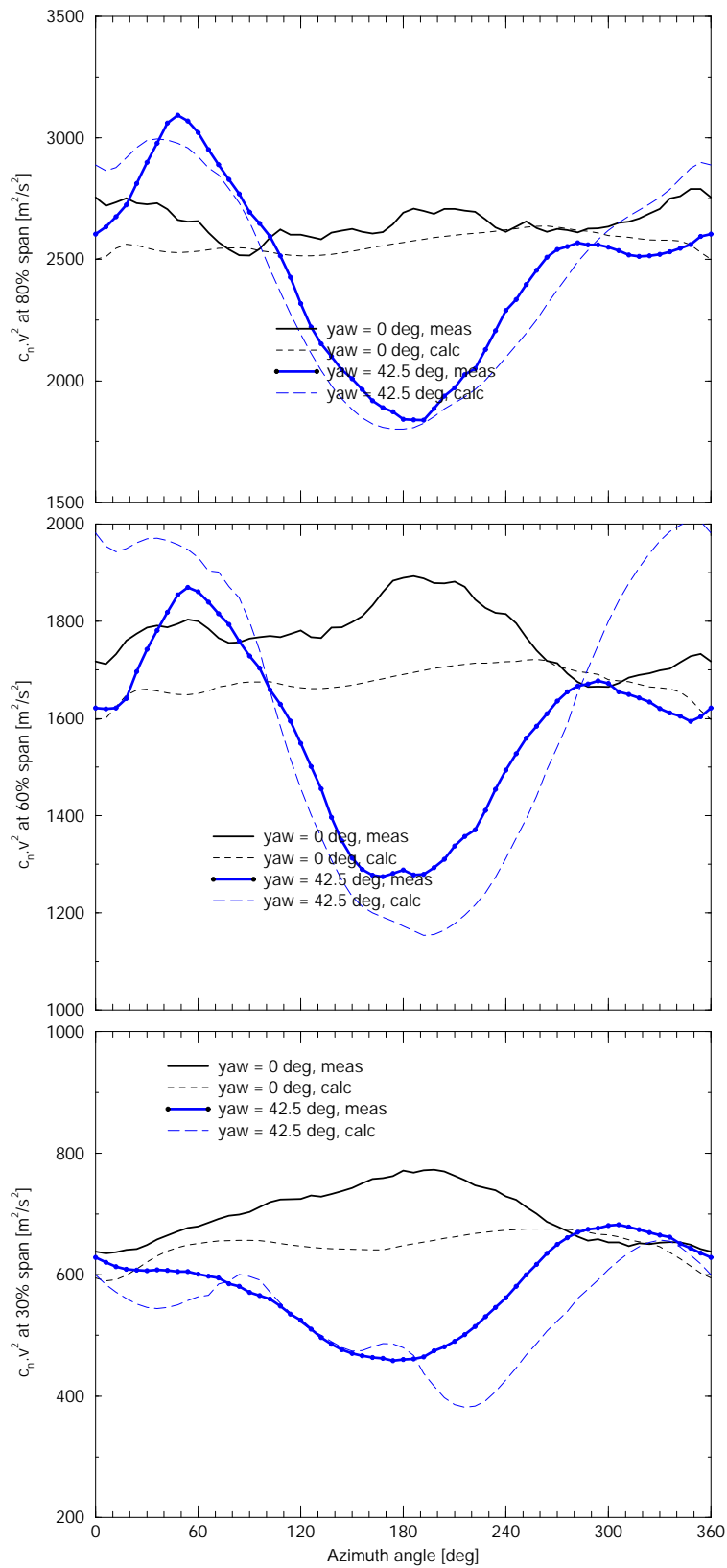


Figure A.10 ECN measurements: $n - \phi_r$ at $\phi_y = 42.5$ deg. and at $a \approx 0.2$; 80% span (top), 60% span, 30% span (bottom)

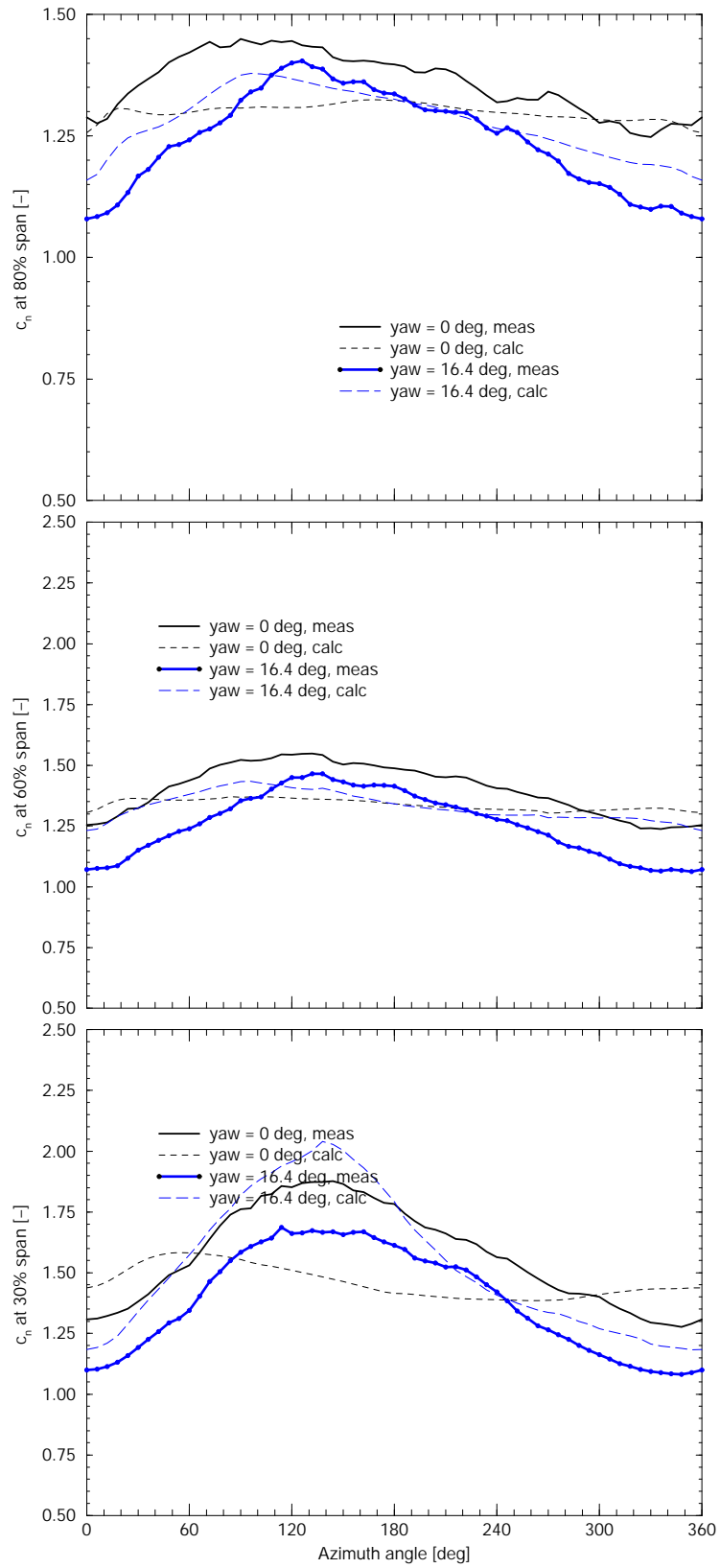


Figure A.11 ECN measurements: $c_n - \phi_r$ at $\phi_y = 16.4$ deg. and at $a \approx 0.3$; 80% span (top), 60% span, 30% span (bottom)

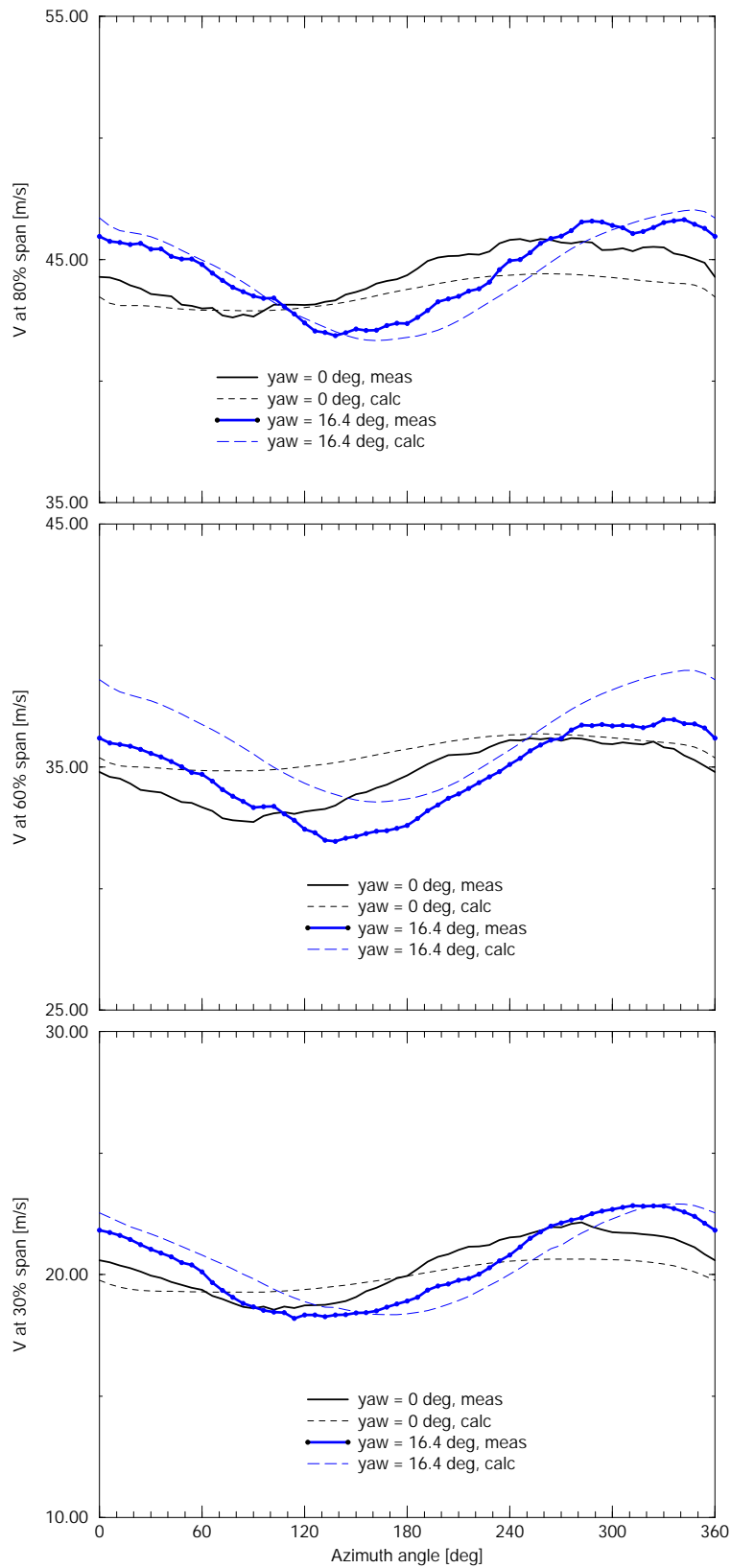


Figure A.12 ECN measurements: $V - \phi_r$ at $\phi_y = 16.4$ deg. and at $a \approx 0.3$; 80% span (top), 60% span, 30% span (bottom)

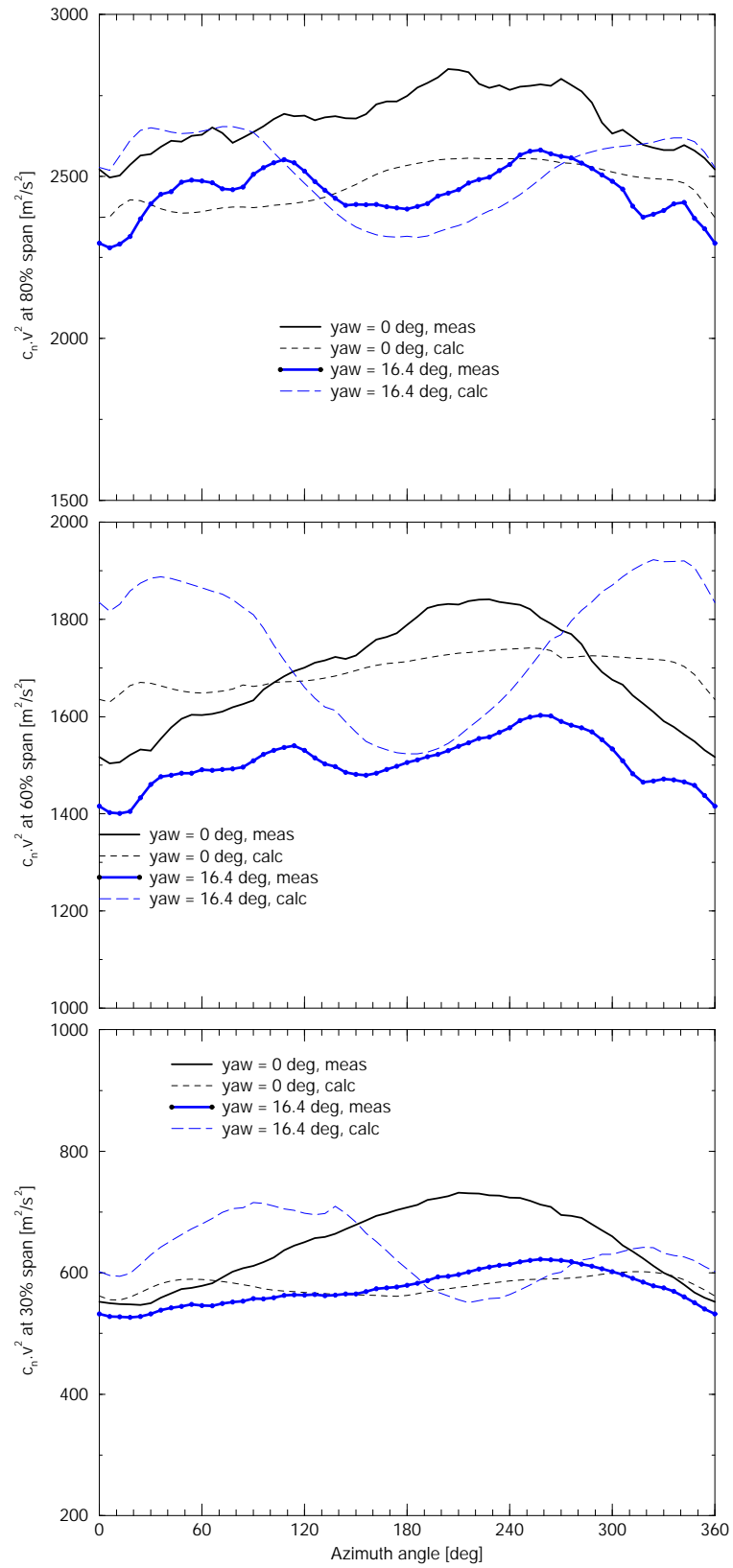


Figure A.13 ECN measurements: $n - \phi_r$ at $\phi_y = 16.4$ deg. and at $a \approx 0.3$; 80% span (top), 60% span, 30% span (bottom)

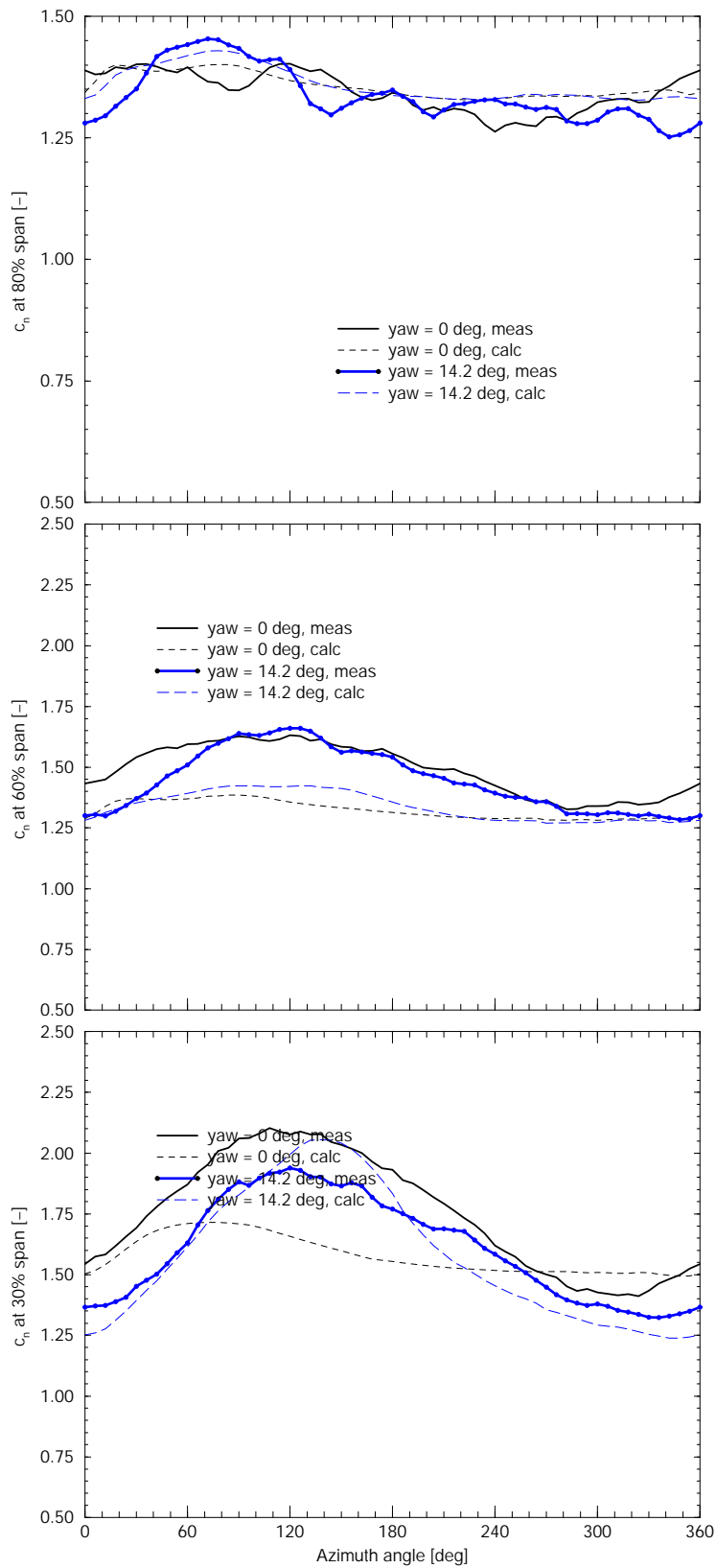


Figure A.14 ECN measurements: $c_n - \phi_r$ at $\phi_y = 14.2$ deg. and at $a \approx 0.2$; 80% span (top), 60% span, 30% span (bottom)

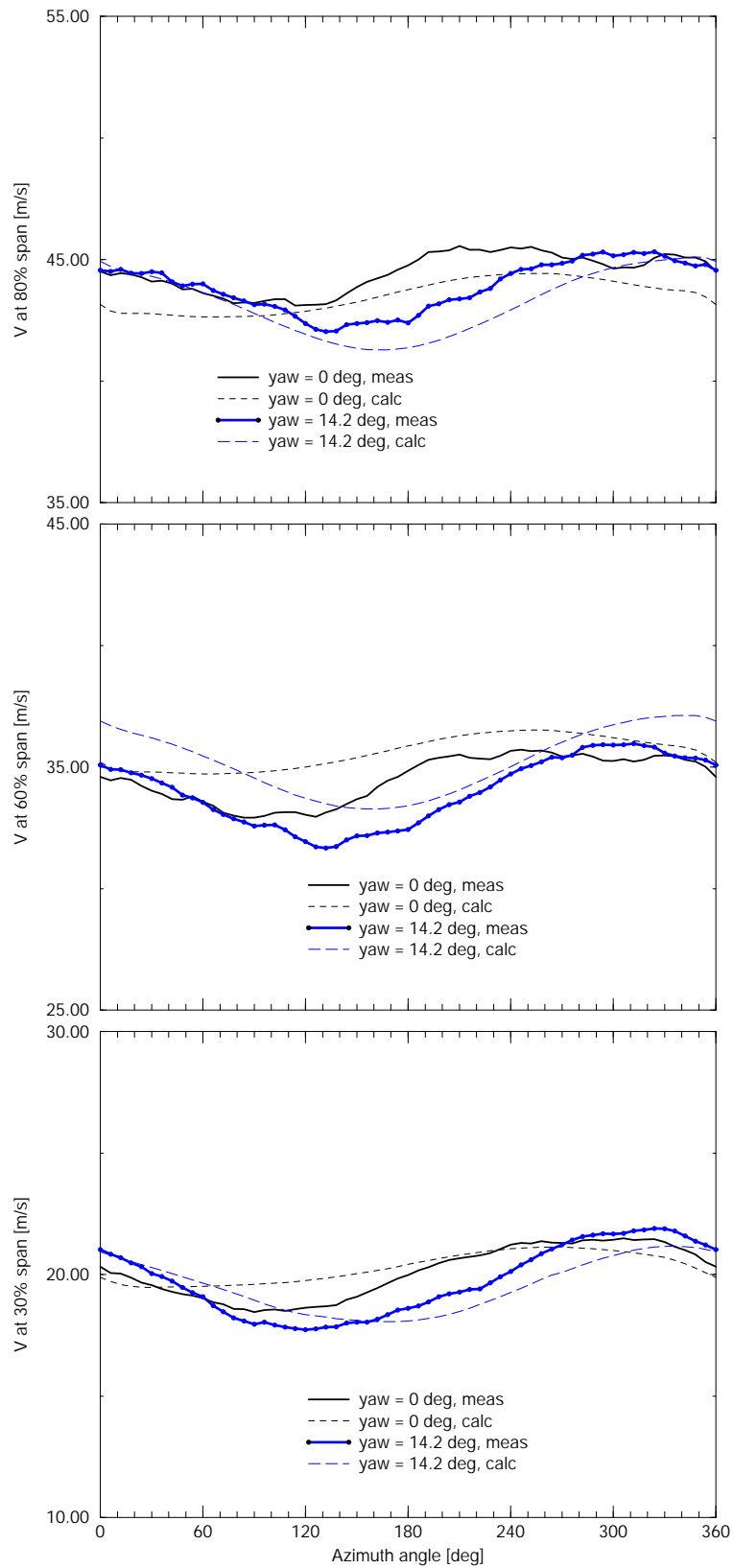


Figure A.15 ECN measurements: $V - \phi_r$ at $\phi_y = 14.2$ deg. and at $a \approx 0.2$; 80% span (top), 60% span, 30% span (bottom)

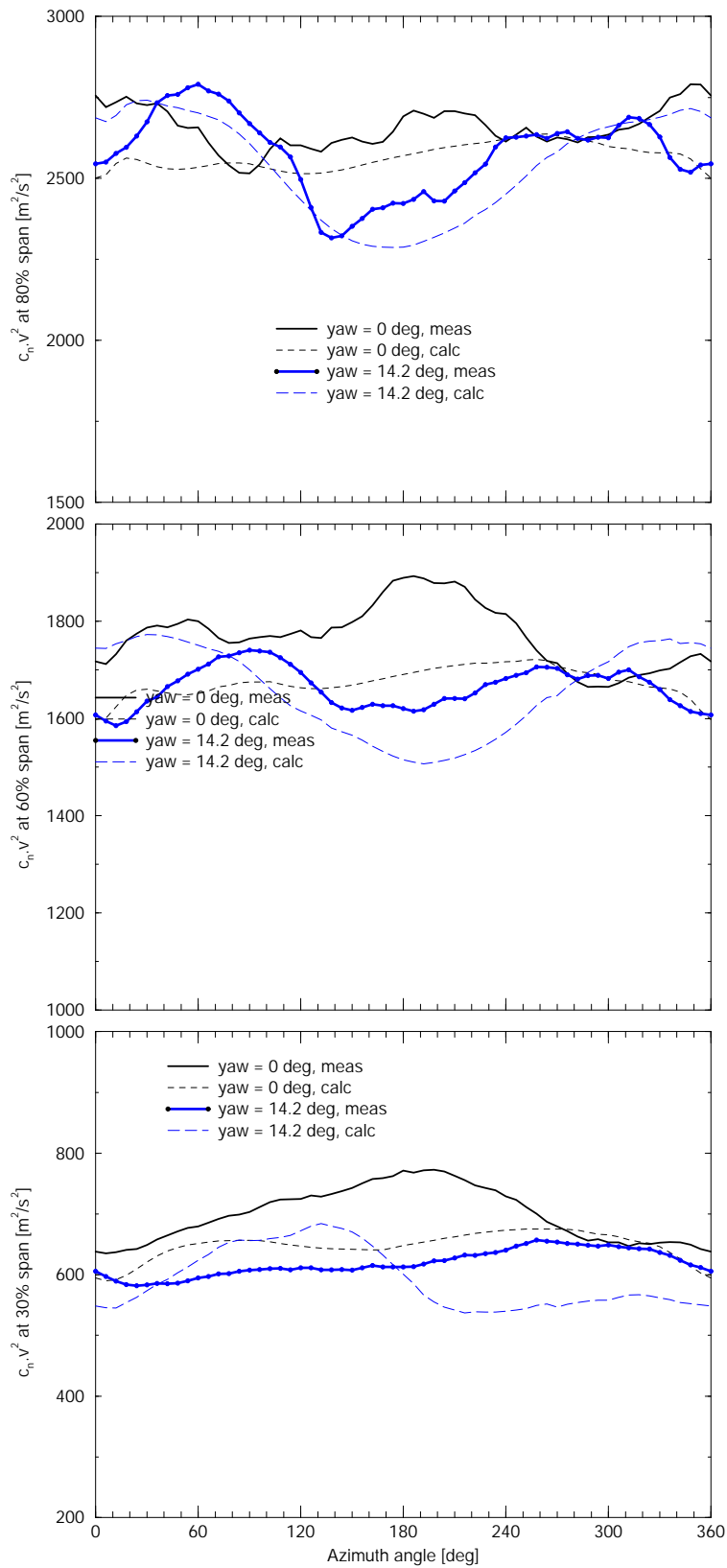


Figure A.16 ECN measurements: $n - \phi_r$ at $\phi_y = 14.2$ deg. and at $a \approx 0.2$; 80% span (top), 60% span, 30% span (bottom)

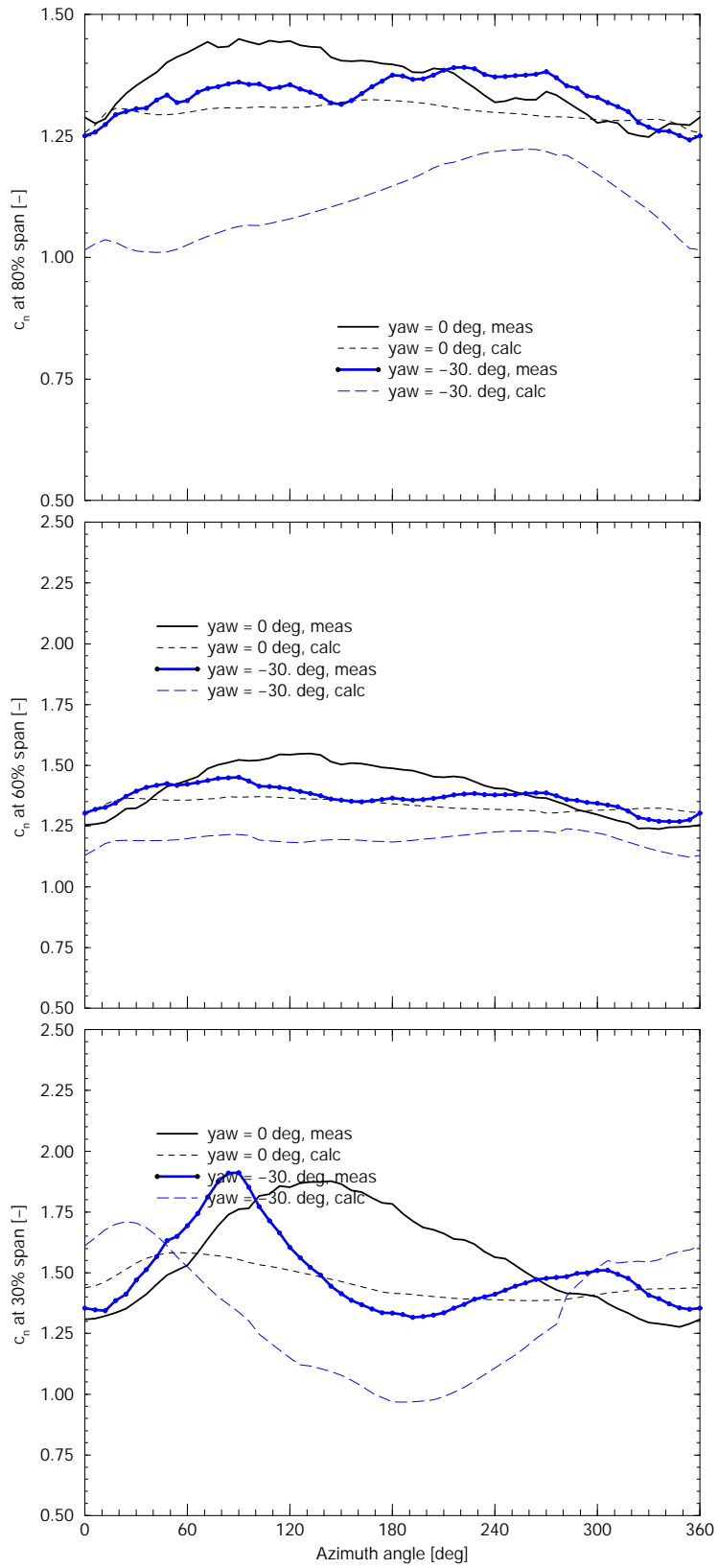


Figure A.17 ECN measurements: $c_n - \phi_r$ at $\phi_y = -30$ deg. and at $a \approx 0.2$; 80% span (top), 60% span, 30% span (bottom)

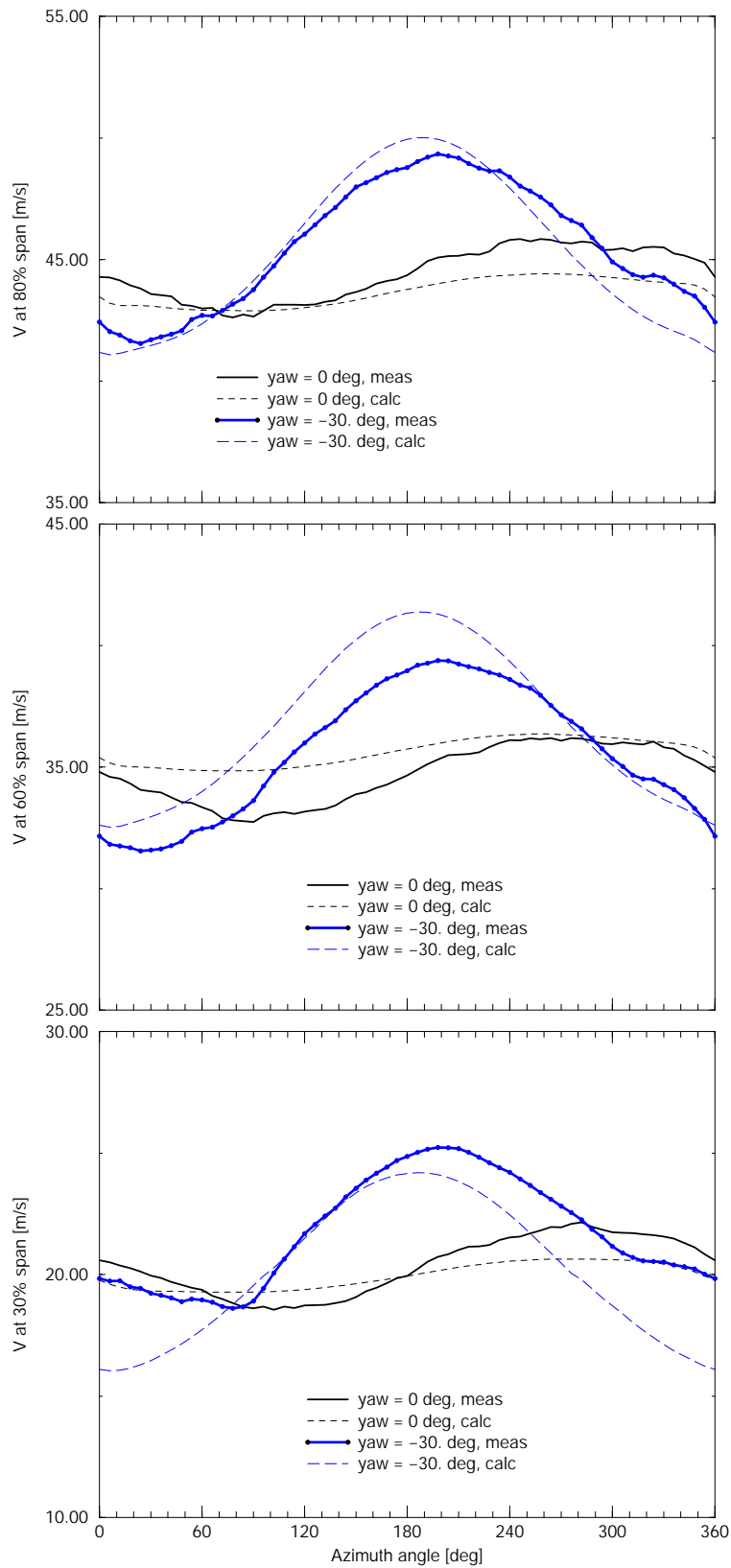


Figure A.18 ECN measurements: $V - \phi_r$ at $\phi_y = -30$ deg. and at $a \approx 0.2$; 80% span (top), 60% span, 30% span (bottom)

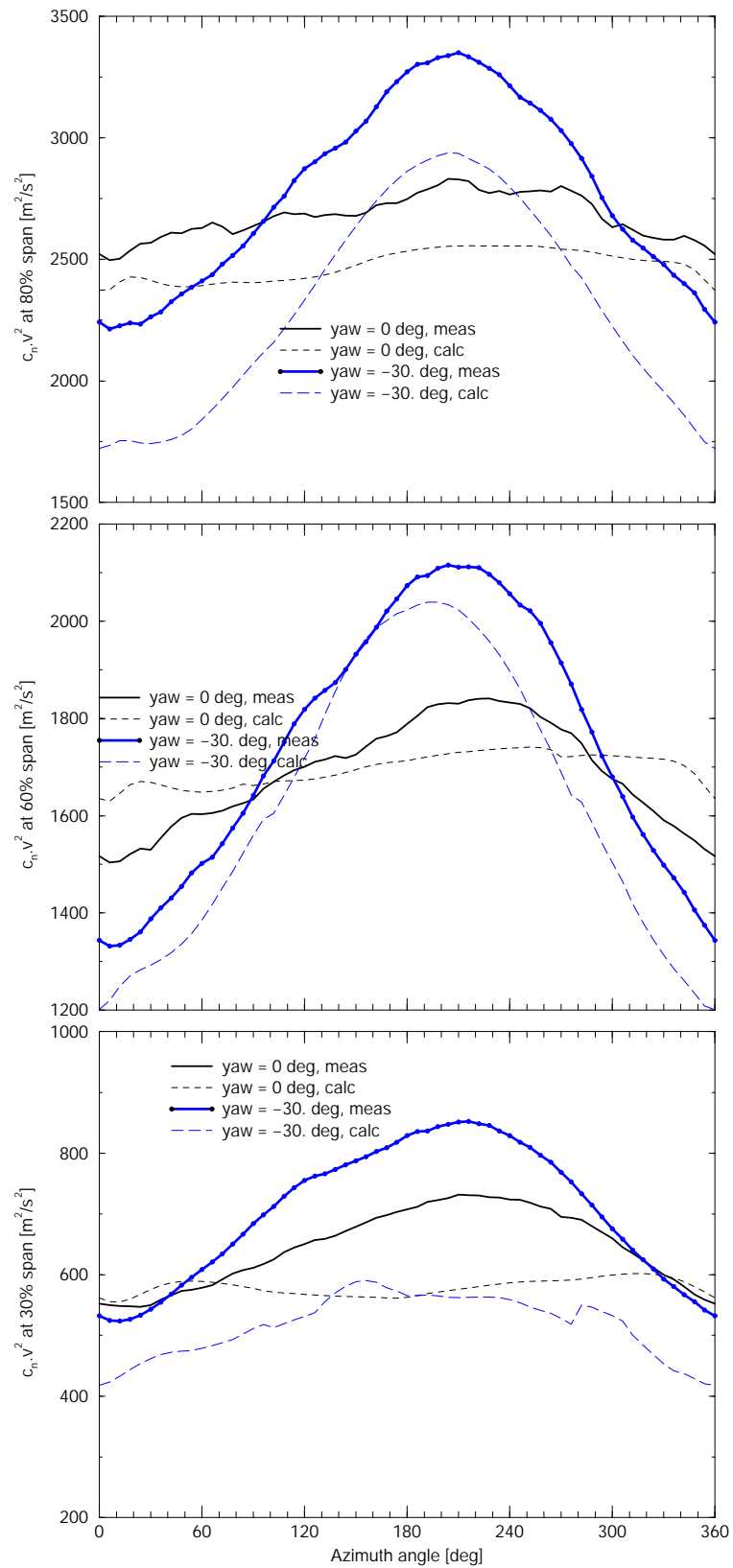


Figure A.19 ECN measurements: $n - \phi_r$ at $\phi_y = -30$ deg. and at $a \approx 0.2$; 80% span (top), 60% span, 30% span (bottom)

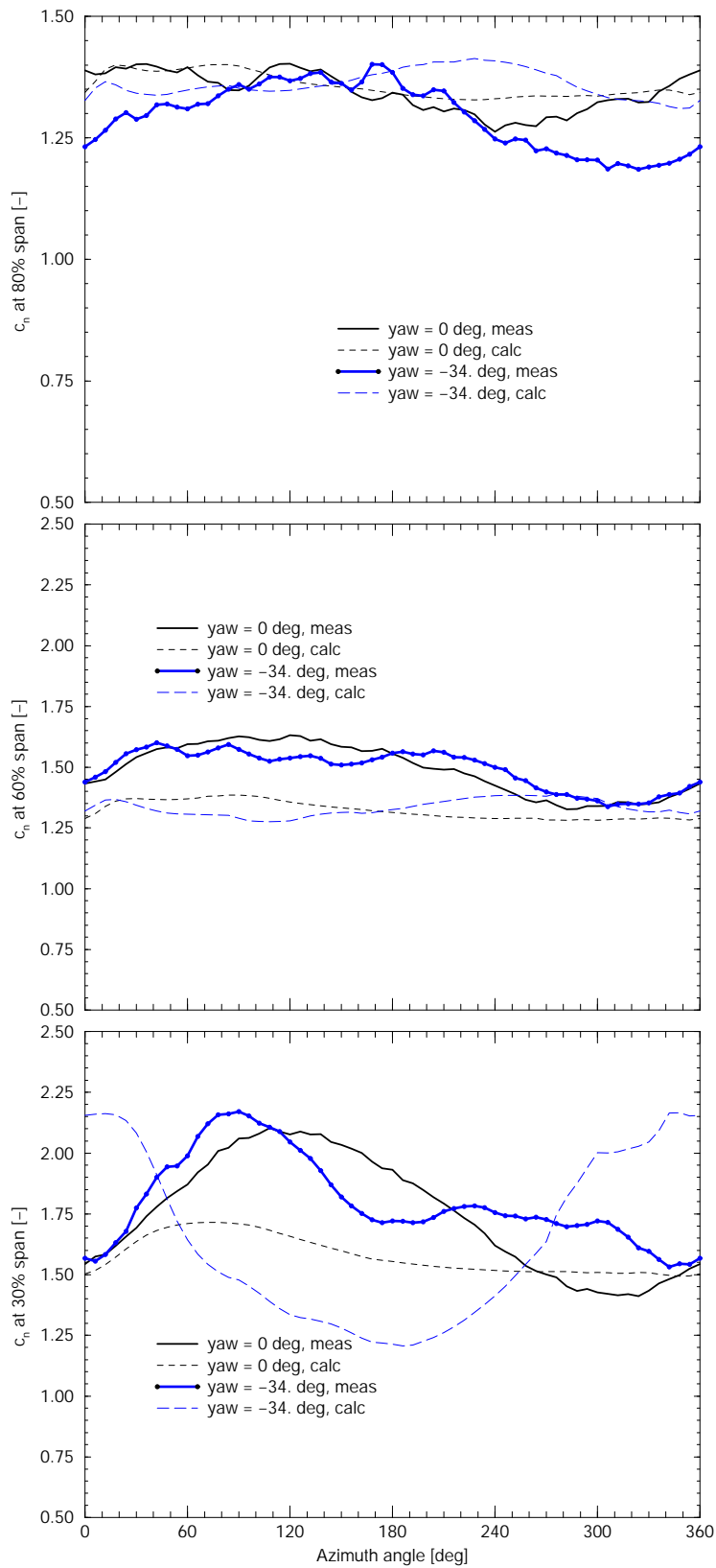


Figure A.20 ECN measurements: $c_n - \phi_r$ at $\phi_y = -34$ deg. and at $a \approx 0.2$; 80% span (top), 60% span, 30% span (bottom)

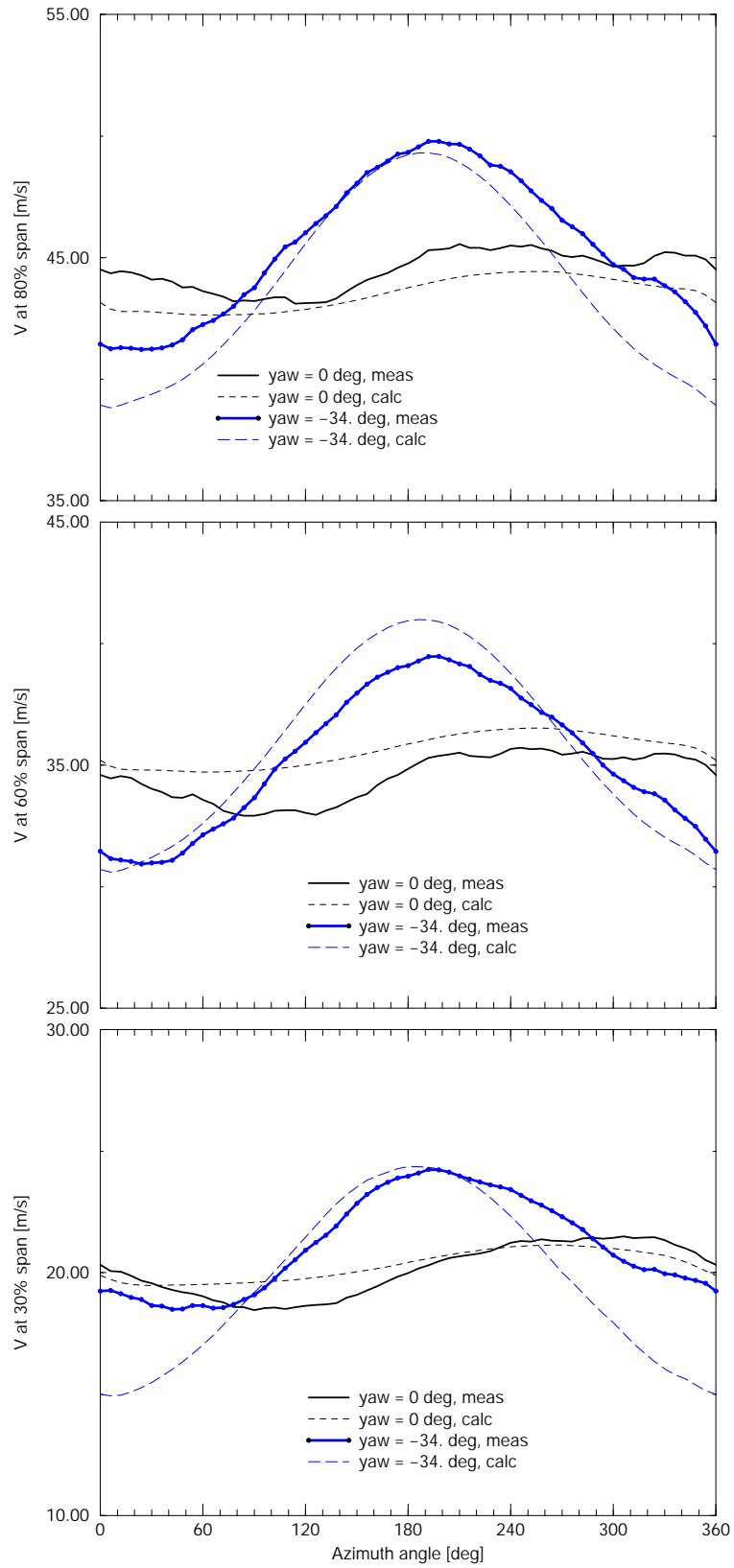


Figure A.21 ECN measurements: $V - \phi_r$ at $\phi_y = -34$ deg. and at $a \approx 0.2$; 80% span (top), 60% span, 30% span (bottom)

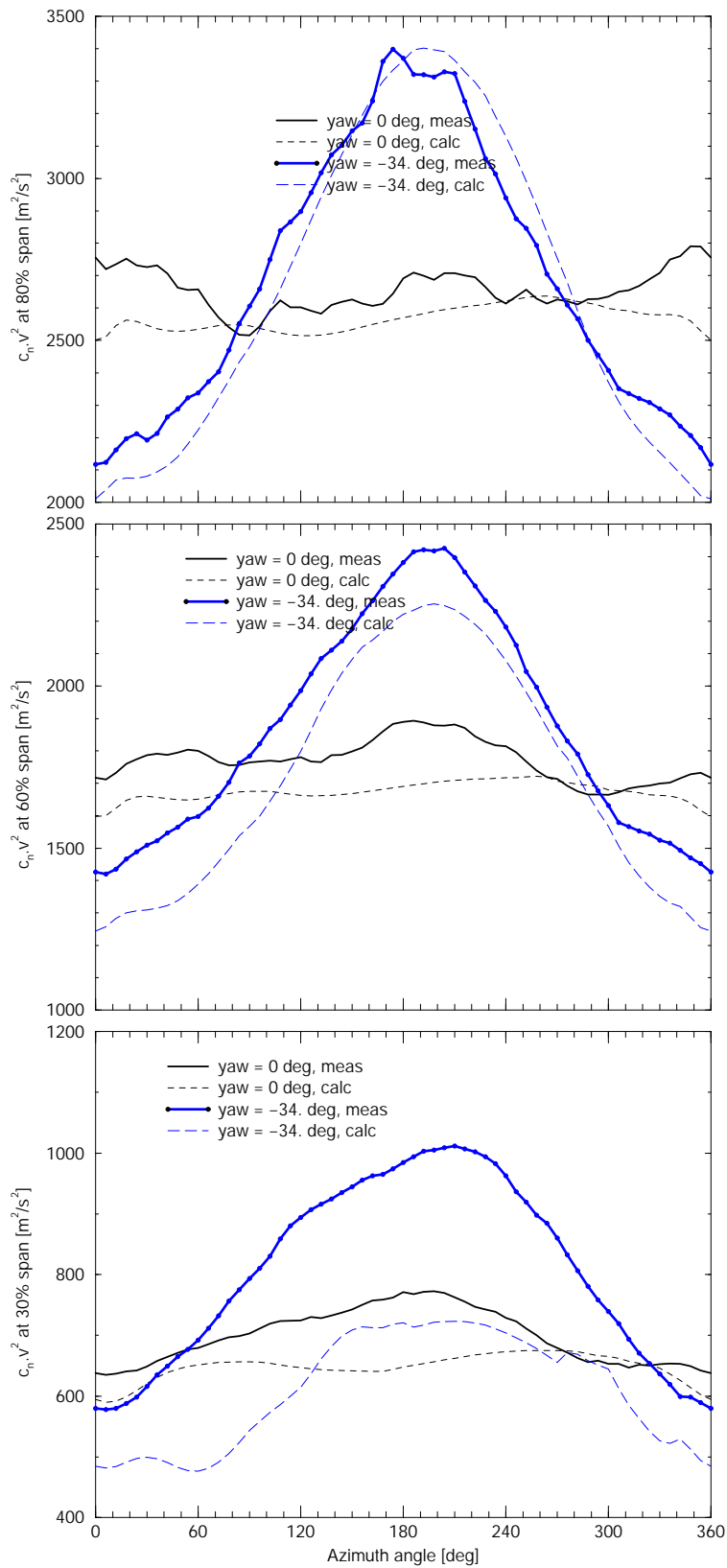


Figure A.22 ECN measurements: $n - \phi_r$ at $\phi_y = -34^\circ$ and at $a \approx 0.2$; 80% span (top), 60% span, 30% span (bottom)

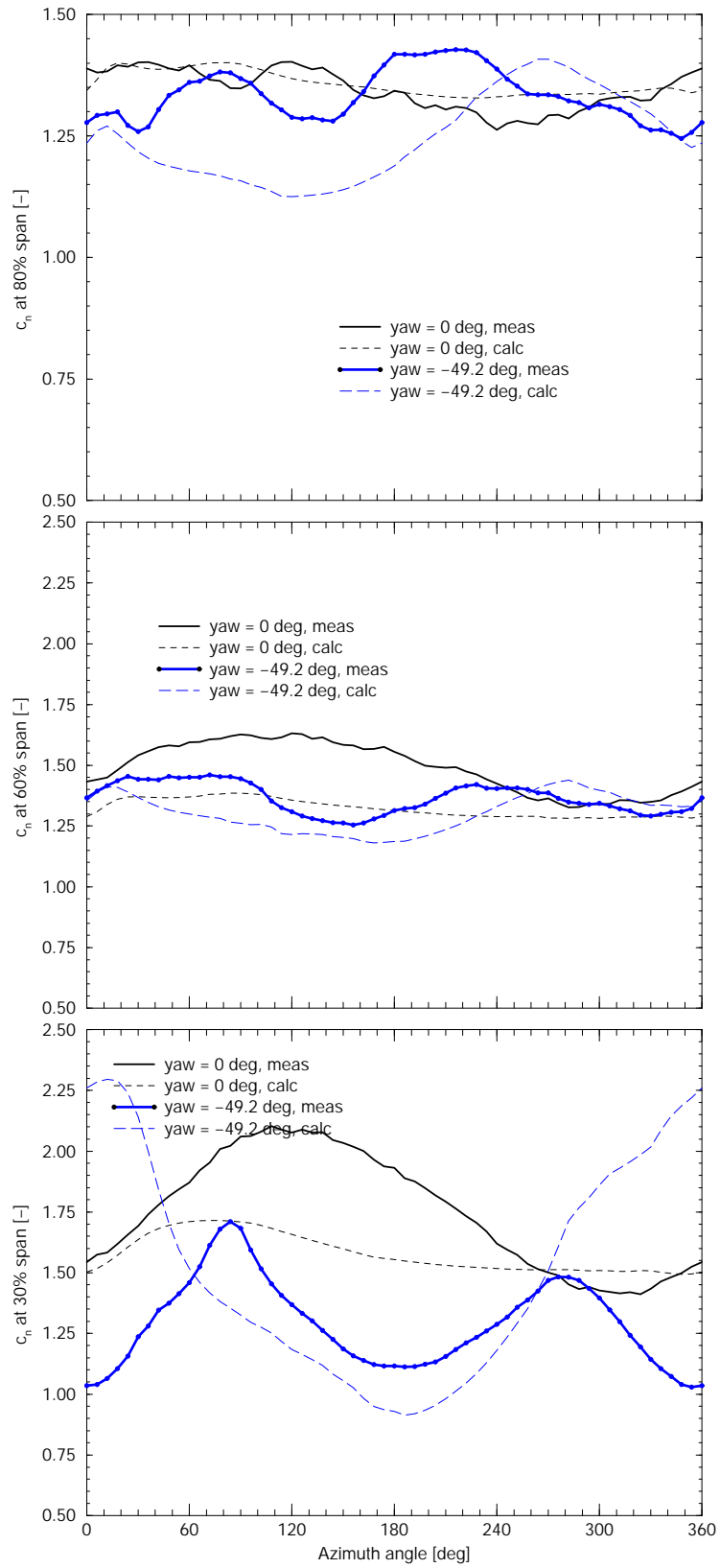


Figure A.23 ECN measurements: $c_n - \phi_r$ at $\phi_y = -49$ deg. and at $a \approx 0.2$; 80% span (top), 60% span, 30% span (bottom)

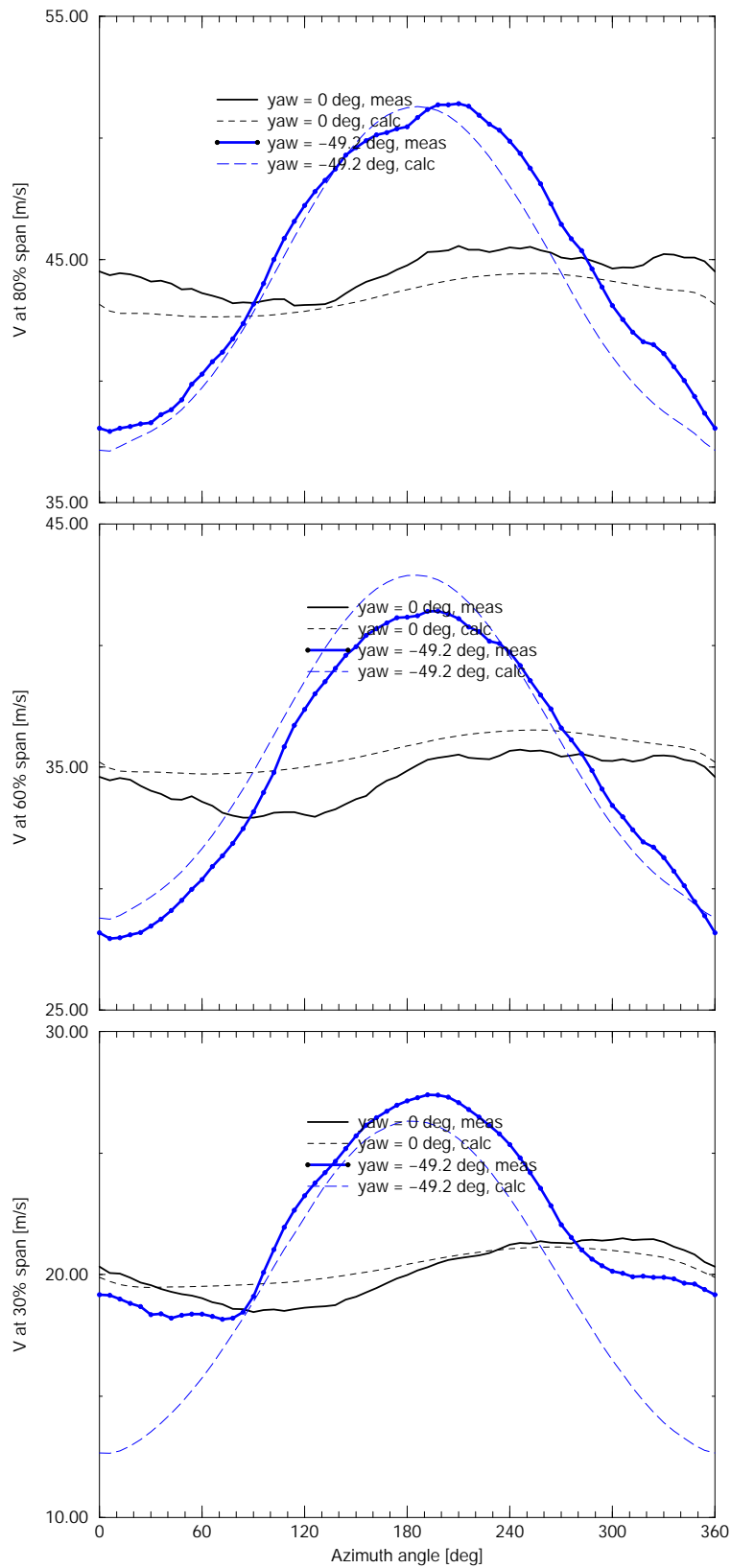


Figure A.24 ECN measurements: $V - \phi_r$ at $\phi_y = -49$ deg. and at $a \approx 0.2$; 80% span (top), 60% span, 30% span (bottom)

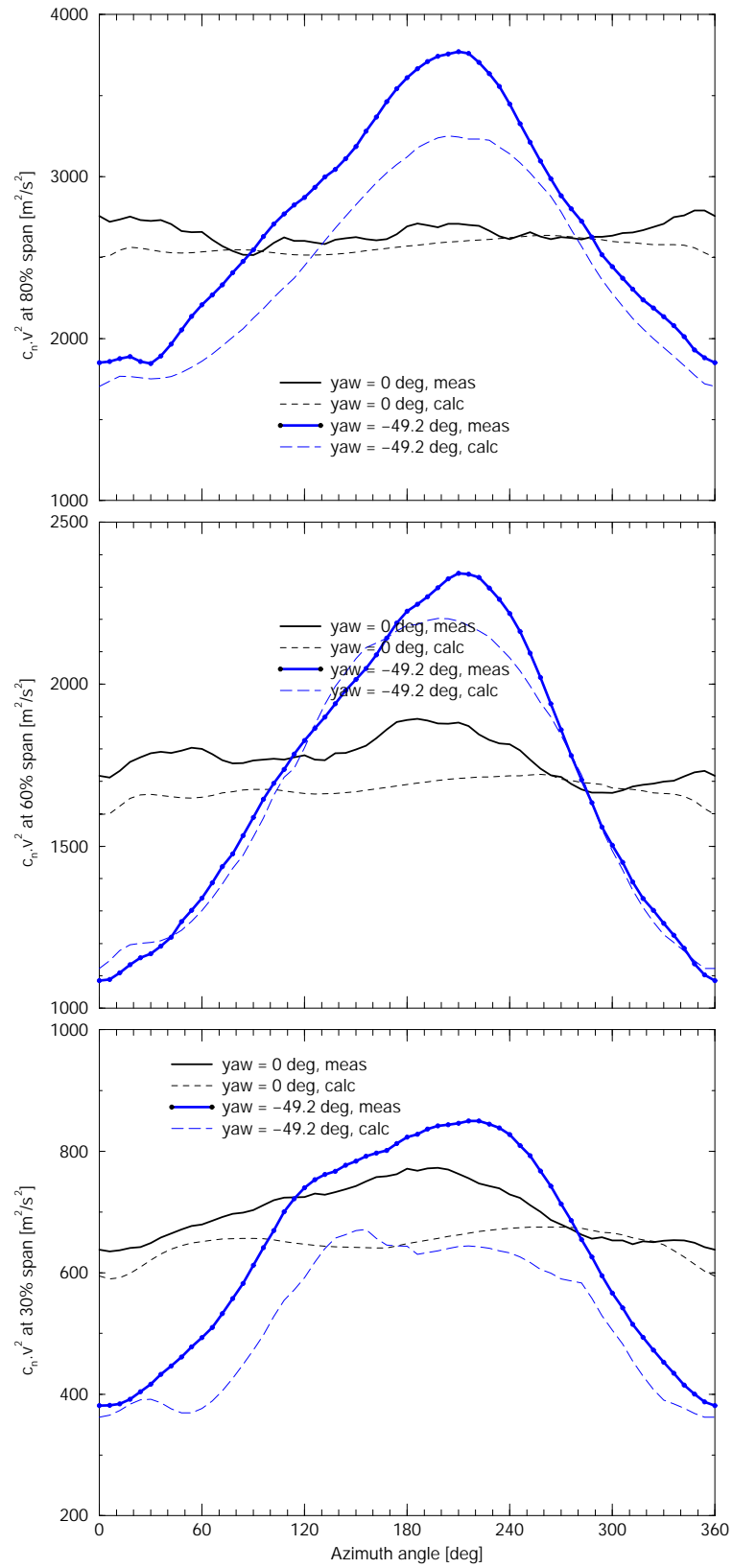


Figure A.25 ECN measurements: $n - \phi_r$ at $\phi_y = -49$ deg. and at $a \approx 0.2$; 80% span (top), 60% span, 30% span (bottom)

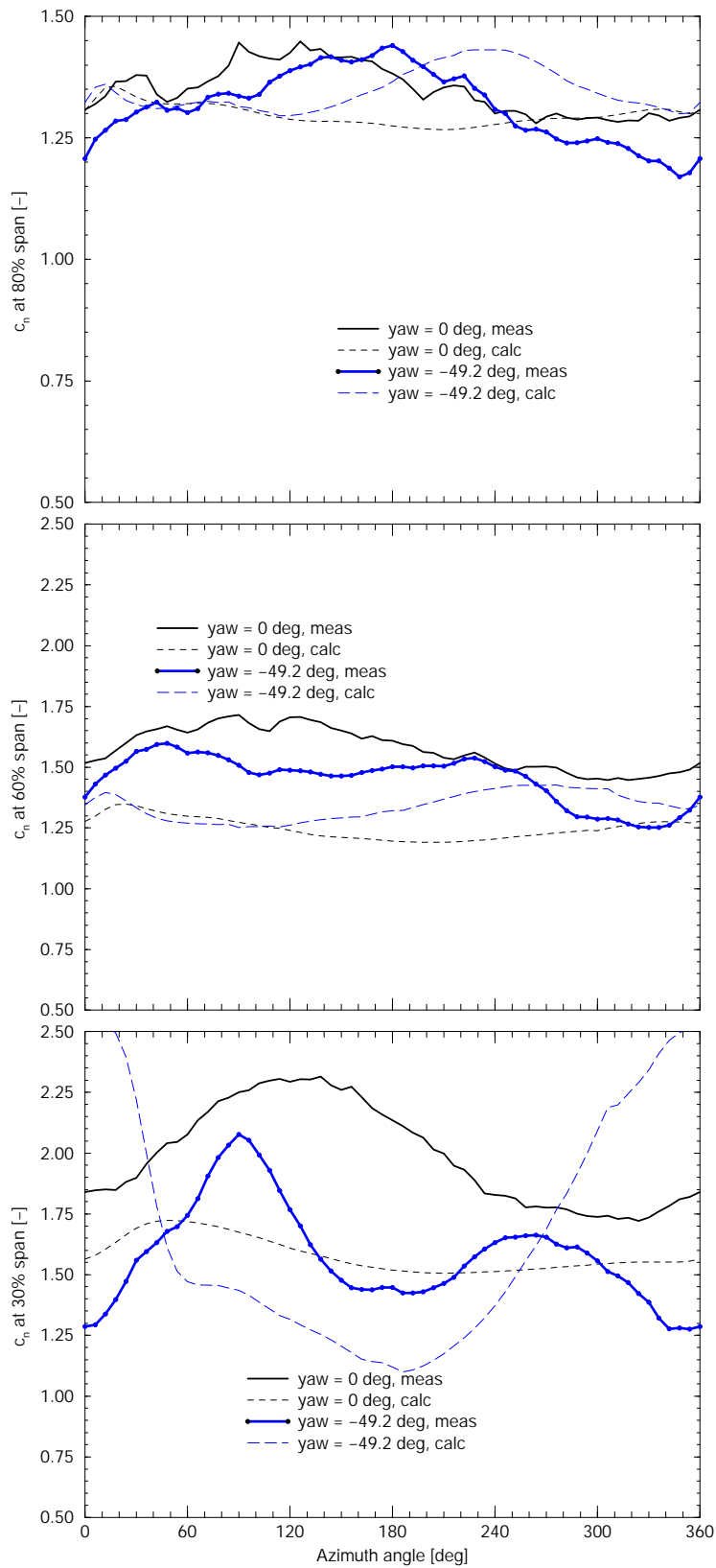


Figure A.26 ECN measurements: $c_n - \phi_r$ at $\phi_y = -49$ deg. and at $a \approx 0.2$; 80% span (top), 60% span, 30% span (bottom)

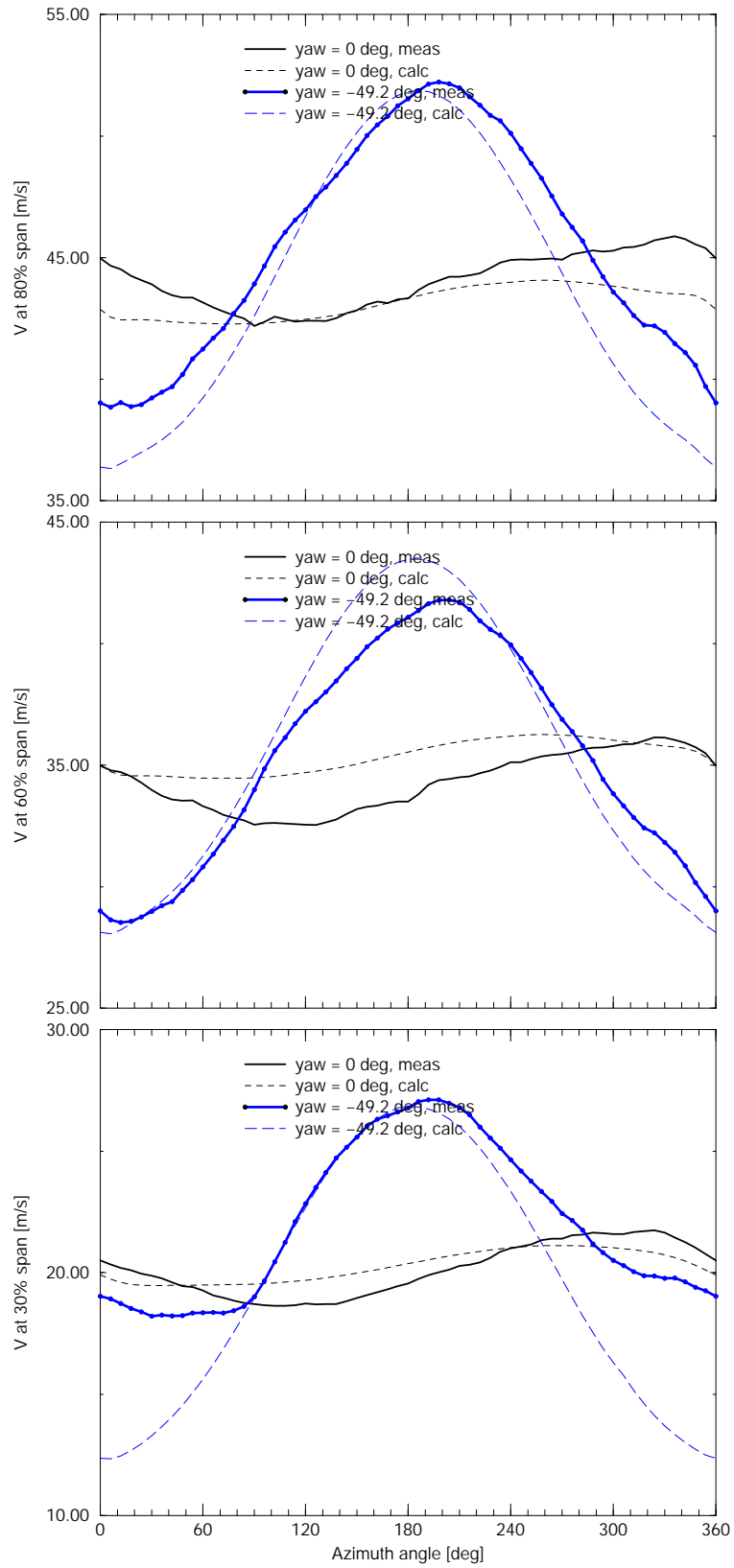


Figure A.27 ECN measurements: $V - \phi_r$ at $\phi_y = -49$ deg. and at $a \approx 0.2$; 80% span (top), 60% span, 30% span (bottom)

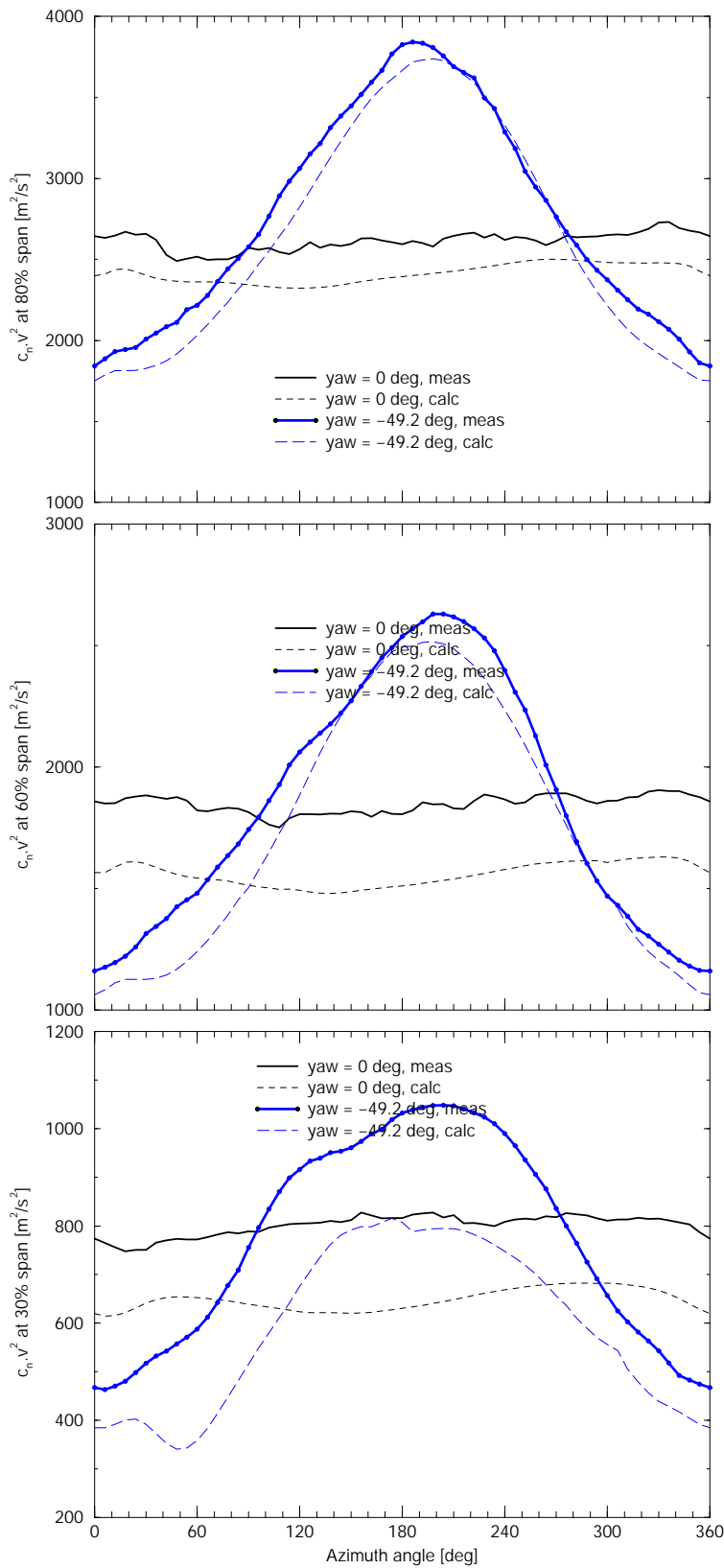


Figure A.28 ECN measurements: $n - \phi_r$ at $\phi_y = -49$ deg. and at $a \approx 0.2$; 80% span (top), 60% span, 30% span (bottom)

EXECUTIVE SUMMARY

Yaw measurements and yaw modelling

Modelling of yawed conditions is known to be one of the major deficiencies in current wind turbine design codes. In the past, large discrepancies have been found in the prediction of mechanical loads at yawed conditions and in particular the prediction of yawing moments (and stability) suffered from large uncertainties, see [1] and [2].

The present report describes an analysis of aerodynamic measurements on wind turbines at yawed conditions. Among others, a comparison is made with calculational results from ECN's wind turbine design code PHATAS-IV.

The measurements which are analysed originate from the database of IEA Annex XVIII, see

<http://www.ecn.nl/wind/other/IEA/index.en.html> and [3].

In this IEA Annex, the aerodynamic measurement programs of different institutes were coordinated. In these measurement programs, the local aerodynamic forces (normal and tangential to the chord) and the associated pressure distributions at different spanwise locations along a wind turbine blade are measured.

The main emphasis in the investigation was on the prediction of the yawing stability (or more specific: the variation of wind turbine loads over the rotor plane). This stability is partly determined by the variation of the induced velocity over the rotorplane, caused by the skewed wake geometry. The variation in induced velocities yields a load unbalance between the upwind and downwind side of the rotorplane and as such a yawing moment.

Until 1990, wind turbine design codes did not predict this load unbalance and resulting yawing moments at all. Yawed conditions were only modelled through the so-called advancing and retreating blade effect, which basically adds or subtracts the tangential free wind speed component to the rotational speed. This results in a symmetric load distribution along the vertical line in the rotorplane. Such load distribution yields a neutral yawing moment, where it was known from measurements that the real yawing moment is stabilizing (i.e. restoring).

This was one of the reasons to perform the EU Joule projects on Dynamic Inflow (see [1] and [2]) in the period 1990-1995. In these projects, the variation of the induced velocity over the rotorplane, was included, based on models from helicopter theory. The models basically assumed a sinusoidal variation of the inflow velocity with the maximum velocity at the upwind side of the rotorplane. Such inflow distribution generally led to a stabilizing yawing moment which was already a considerable improvement compared to the previously used 'advancing and retreating models'.

However, the results of a Dutch national project, performed in 1998, showed these sinusoidal models to be deficient as well. In that project, see [8], a model rotor was placed in the wind tunnel of the University of Delft and direct measurements of the inflow distribution in its rotorplane were made. The measurements have been used to improve the yaw model in the PHATAS code. It was found that the real inflow distribution differs considerably from the expected sinusoidal distribution. This was in particular true near the root of a blade where the root vorticity even makes the maximum velocity to occur at the downwind side of the rotorplane. This then

tends to destabilize the yawing moment. Obviously the inflow measurements from [8] only gave indirect information on the load distribution. Non-linear aerodynamic effects, but also the advancing and retreating blade effect as well as flexibilities, wind shear, tilt angle, etc make the relation between the inflow variation and the load variation less straightforward. Therefore a direct validation of the load variation at yawed conditions is extremely useful. The IEA Annex XVIII measurements offer the material for such validation. The main aim of the present analysis has therefore been to investigate whether the root can contribute to a destabilizing yawing moment where at the same time the tip can contribute to a stabilizing yawing moment.

Results and conclusions

A number of IEA Annex XVIII measurements have been selected for further analysis. The campaigns should fulfill the following criteria:

1. The campaign should be taken at a substantial (mean) yaw angle (> 15 degrees);
2. The averaged axial induction factor (which obviously only can be derived from calculations) should be ≥ 0.15 . At lower axial induction factors the loading variation over the rotor plane is mainly determined by the advancing and retreating blade effect;
3. The wind shear should be measured. This is an important requirement because the loading variation over the rotorplane interferes with the variation which is caused by wind shear and their effects are difficult to distinguish;
4. Preferably the yawed campaign should be compared with a similar campaign at (almost) zero yaw.

The aerodynamic normal forces at different radial stations of the selected campaigns have then been binned on azimuth angle and compared with the results from PHATAS-IV. The measurements showed that at the root (i.e. at 30% span) the maximum force was found at the downwind side of the rotorplane, corresponding to a destabilizing yawing moment. At the tip (i.e. at 80% span) the maximum was found at the upwind side of the rotorplane. Generally speaking the PHATAS-IV results show a good agreement with the measured results. Most important is that they also predict the destabilizing yawing moment contribution at the root where at the same time the tip is predicted to contribute a stabilizing yawing moment.

Finally a limited comparison has been made with the newly developed free wake lifting line code AWSM. The AWSM results shows a very good agreement with the measurements at the 80% section, but at the 30% section there were considerable differences. The explanation for these differences have not been found yet.

Date: October 2004

Number of report: ECN-C--04-097

Title Annexlyse: Validation of yaw models, on basis of detailed aerodynamic measurements on wind turbine blades

Author(s) J.G. Schepers

Principal(s) SenterNovem

ECN project number 7.4154

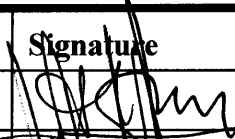
Principal's order number 2020.01.13.10.003

Programme(s) DEN

Abstract

In this report an analysis is made of measured local aerodynamic loads on wind turbine blades at yawed conditions. The measured loads are compared with results from the wind turbine design code PHATAS-IV. The aerodynamic model in PHATAS-IV is based on the blade element momentum model, with correction formula for yawed conditions. The measured data are also compared with the results from the newly developed free wake lifting line model AWMS.

Key words: yaw aerodynamics of wind turbines; validation of wind turbine design codes

Authorization	Name	Signature	Date
Checked	H. Snel		30 nov 04
Approved	H.B Hendriks		30 nov 04
Authorized	C.A.M. van der Klein (manager ECN Windenergie a.i.s)		01-12-04